How to verify the Quark-Gluon Plasma with Gravitational-Wave Detectors

Talk at the Hirschegg Workshop "Neutron Star Mergers:From gravitational waves to nucleosythesis"
Hirschegg (Austria), 16.01.2017

Matthias Hanauske, Kentaro Takami, Luke Bovard, Luciano Rezzolla, Filippo Galeazzi, José A. Font, and Horst Stöcker

Frankfurt Institute for Advanced Studies
Johann Wolfgang Goethe-University
Institute for Theoretical Physics
Department of Relativistic Astrophysics
Frankfurt am Main, Germany

How to verify the Quark-Gluon Plasma with Gravitational-Wave Detectors

1. Introduction
2. Numerical General Relativity
3. Equation of State
   and the Hadron-Quark Phase Transition
4. Internal Properties of Hypermassive Neutron and
   Hybrid Stars in the Post-Merger Phase
5. Outlook and Summary

First observation gravitational waves from binary black hole merger by LIGO

Facts about GW150914
Merger of two black holes of around 36 and 29 solar masses
Distance: 410 Mpc (1340 million Ly)

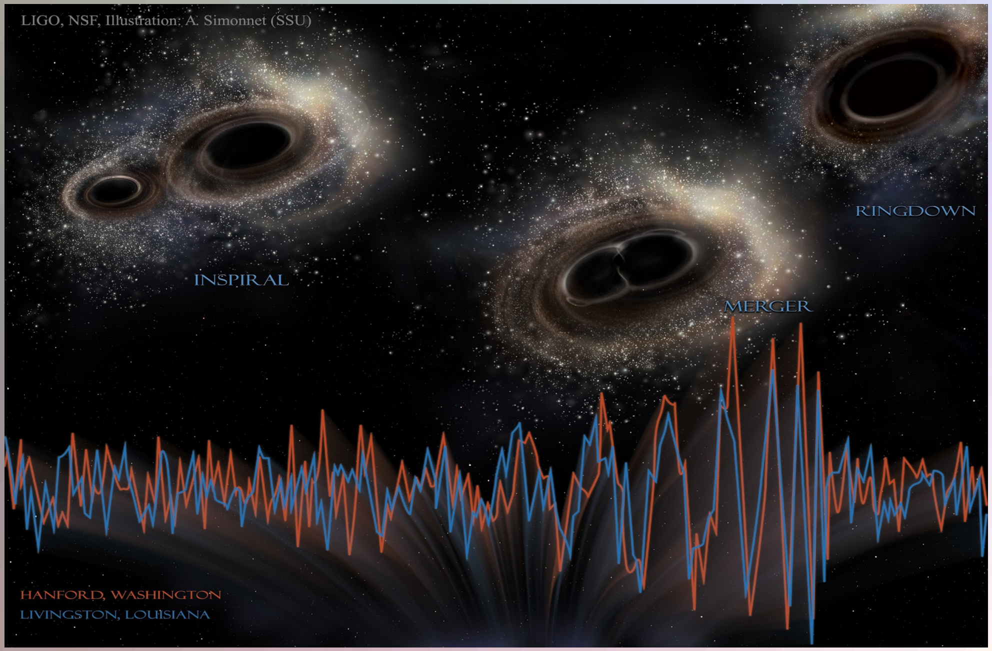

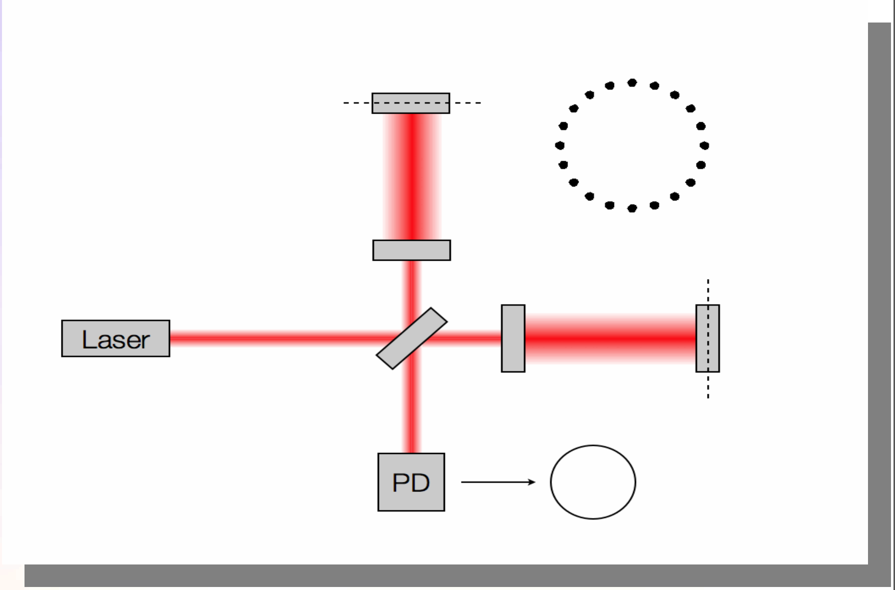

Credit: Les Wade from Kenyon College.

Gravitational Waves from Binary Neutron Star Mergers

Neutron star merger (Simulation)

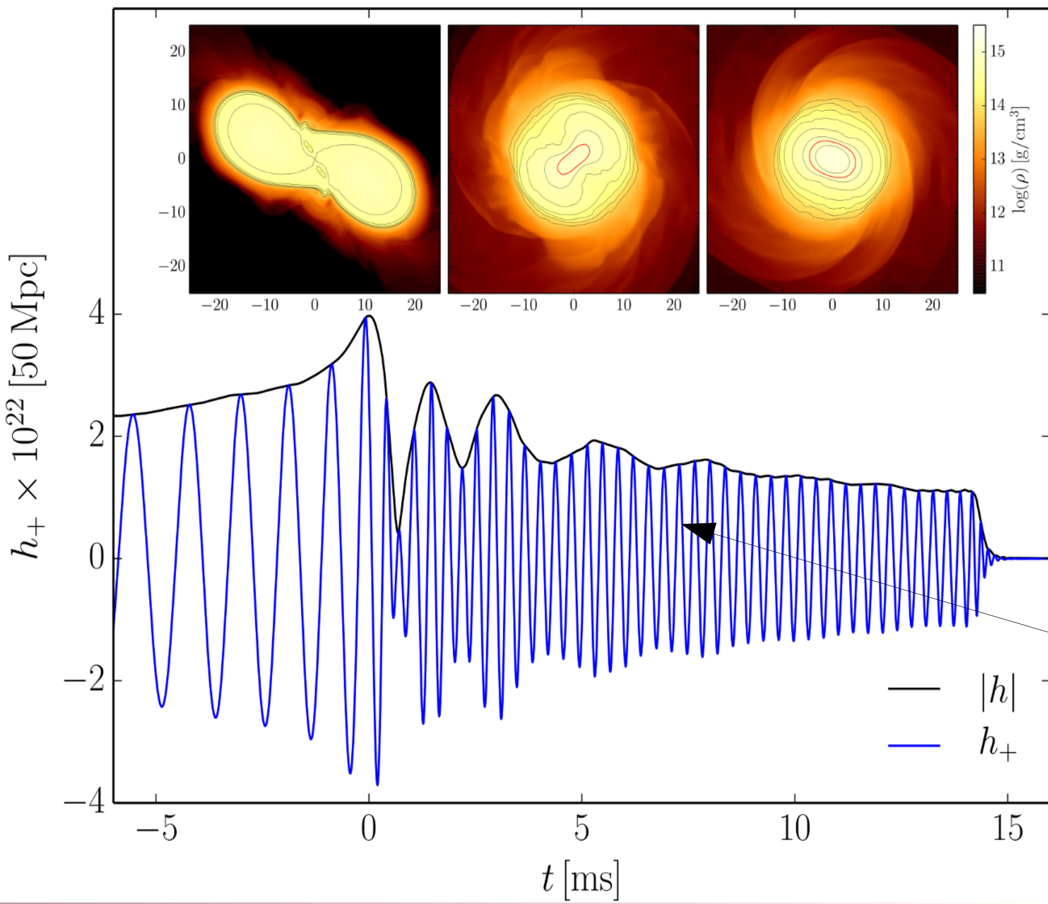

Merger of two Black Holes

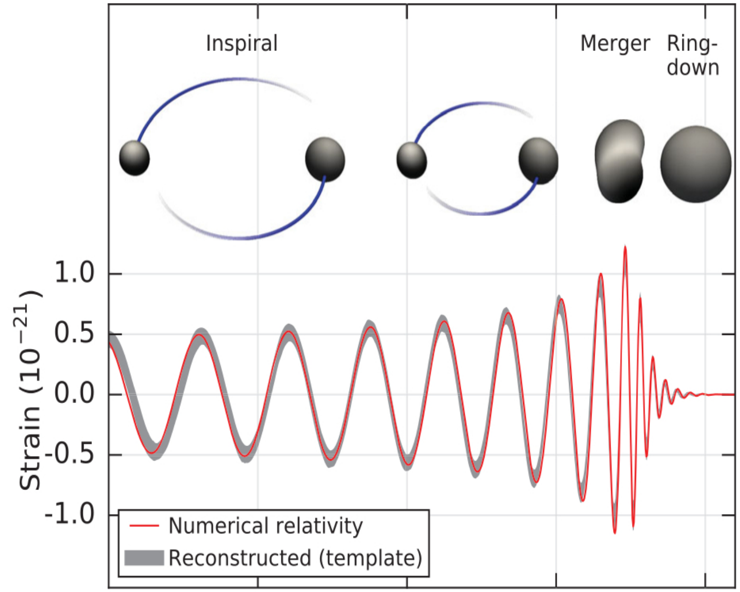

Main Difference:

Neutron star mergers could have a ***post-merger phase***

The Neutron Star Merger Product

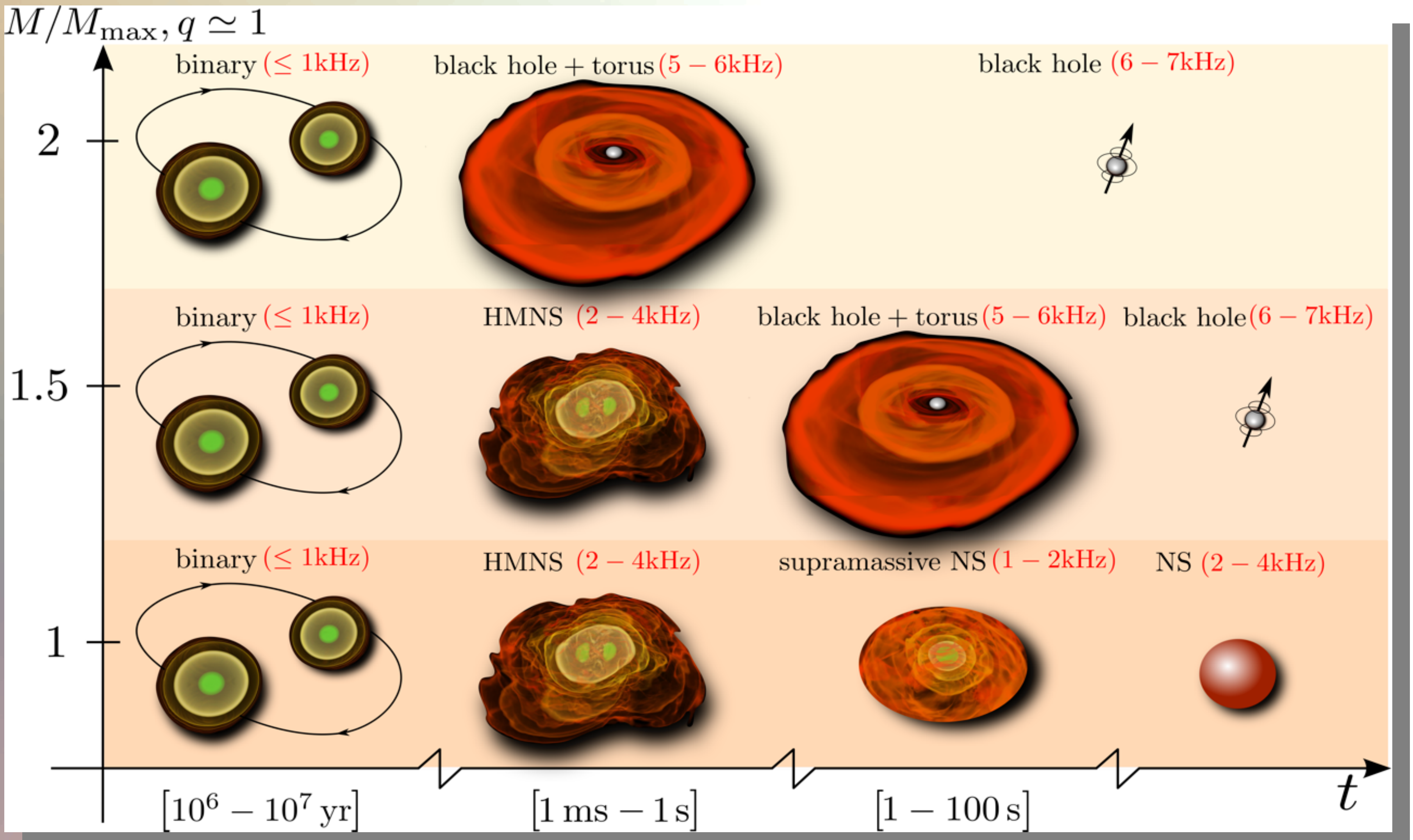

Relativistic Hydrodynamics and Numerical General Relativity

The time evolution of a merger scenario of a binary neutron star system requires the (3+1)-Split of the Einstein- and hydrodynamic equations.

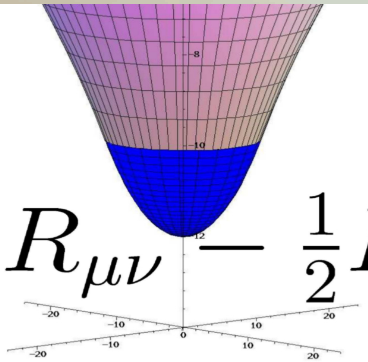

$$\nabla_\mu(\rho u^\mu) = 0\,,$$
$$\nabla_\nu T^{\mu\nu} = 0\,.$$

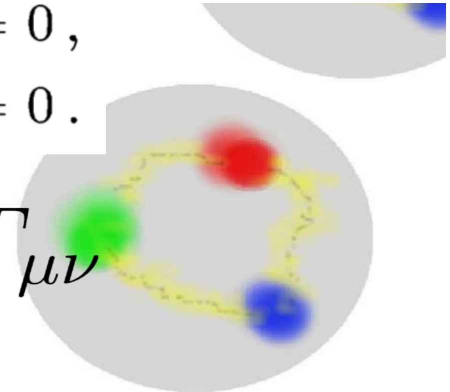

$$R_{\mu\nu} - \frac{1}{2} R\, g_{\mu\nu} = \frac{8\pi G}{c^4} T_{\mu\nu}$$

$$g_{\mu\nu} = \begin{pmatrix} -\alpha^2 + \beta_i\beta^i & \beta_i \\ \beta_i & \gamma_{ij} \end{pmatrix}$$

(3+1) decomposition of spacetime

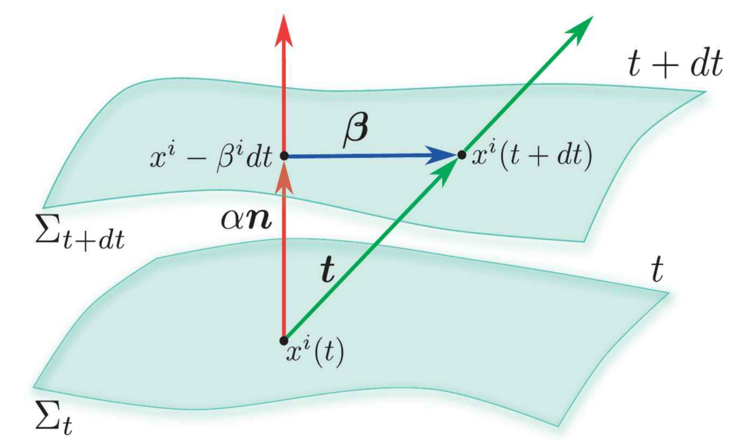

$$d\tau^2 = \alpha^2(t, x^j)dt^2$$

$$x^i_{t+dt} = x^i_t - \beta^i(t, x^j)dt$$

All figures and equations from: Luciano Rezzolla, Olindo Zanotti: Relativistic Hydrodynamics, Oxford Univ. Press, Oxford (2013)

The ADM equations

The ADM (Arnowitt, Deser, Misner) equations come from a reformulation of the Einstein equation using the (3+1) decomposition of spacetime.

$$\begin{aligned}\partial_t \gamma_{ij} &= -2\alpha K_{ij} + \mathscr{L}_{\boldsymbol{\beta}} \gamma_{ij} \\ &= -2\alpha K_{ij} + D_i \beta_j + D_j \beta_i\end{aligned}$$

$$\begin{aligned}\partial_t K_{ij} =& - D_i D_j \alpha + \beta^k \partial_k K_{ij} + K_{ik} \partial_j \beta^k + K_{kj} \partial_i \beta^k \\ &+ \alpha \left({}^{(3)}R_{ij} + K K_{ij} - 2 K_{ik} K^k{}_j \right) + 4\pi\alpha \left[\gamma_{ij} (S - E) - 2S_{ij}) \right]\end{aligned}$$

Time evolving part of ADM

$$D_j (K^{ij} - \gamma^{ij} K) = 8\pi S^i$$

$${}^{(3)}R + K^2 - K_{ij} K^{ij} = 16\pi E$$

Constraints on each hypersurface

Three dimensional covariant derivative

$$D_\nu := \gamma^\mu{}_\nu \nabla_\mu = (\delta^\mu_\nu + n_\nu n^\mu) \nabla_\mu$$

Three dimensional Riemann tensor

$${}^{(3)}R^\mu{}_{\nu\kappa\sigma} = \partial_\kappa {}^{(3)}\Gamma^\mu_{\nu\sigma} - \partial_\sigma {}^{(3)}\Gamma^\mu_{\nu\kappa} + {}^{(3)}\Gamma^\mu_{\lambda\kappa} {}^{(3)}\Gamma^\lambda_{\nu\sigma} - {}^{(3)}\Gamma^\mu_{\lambda\sigma} {}^{(3)}\Gamma^\lambda_{\nu\kappa}$$

$${}^{(3)}\Gamma^\alpha_{\beta\gamma} = \frac{1}{2} \gamma^{\alpha\delta} \left(\partial_\beta \gamma_{\gamma\delta} + \partial_\gamma \gamma_{\delta\beta} - \partial_\delta \gamma_{\beta\gamma} \right)$$

Spatial and normal projections of the energy-momentum tensor:

$$\begin{aligned} S_{\mu\nu} &:= \gamma^\alpha{}_\mu \, \gamma^\beta{}_\nu T_{\alpha\beta} \,, \\ S_\mu &:= -\gamma^\alpha{}_\mu \, n^\beta T_{\alpha\beta} \,, \\ S &:= S^\mu{}_\mu \,, \\ E &:= n^\alpha \, n^\beta T_{\alpha\beta} \,, \end{aligned}$$

Extrinsic Curvature:

$$K_{\mu\nu} := -\gamma^\lambda{}_\mu \nabla_\lambda n_\nu$$

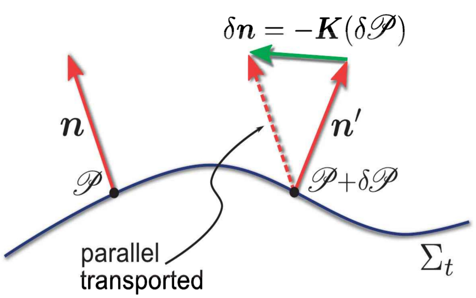

All figures and equations from: Luciano Rezzolla, Olindo Zanotti: Relativistic Hydrodynamics, Oxford Univ. Press, Oxford (2013)

General Relativity and Quantum Cromodynamics

ART	Yang-Mills-Theories
$D_\beta v^\alpha = \partial_\beta\, v^\alpha + \Gamma^\alpha_{\sigma\beta}\, v^\sigma$	$D_{\beta a}{}^b = \partial_\beta\, 1_a{}^b + ig\, A_{\beta a}{}^b$
$R^\delta{}_{\mu\alpha\beta}\, v^\mu = [D_\alpha, D_\beta]\, v^\delta$ $R^\delta{}_{\mu\alpha\beta} = \Gamma^\delta_{\mu\alpha\|\beta} - \Gamma^\delta_{\mu\beta\|\alpha} + \Gamma^\delta_{\nu\beta}\Gamma^\nu_{\mu\alpha} + \Gamma^\delta_{\nu\alpha}\Gamma^\nu_{\mu\beta}$	$F_{\alpha\beta a}{}^b = \frac{1}{ig}\left[D_{\alpha a}{}^c, D_{\beta c}{}^b\right]$ $= A_{\beta a}{}^b{}_{\|\alpha} - A_{\alpha a}{}^b{}_{\|\beta} + \frac{1}{ig}\left[A_{\alpha a}{}^c, A_{\beta c}{}^b\right]$
$\mathcal{L}_G = R + \underbrace{(c_1\, R_{\mu\nu}R^{\mu\nu} + \ldots)}_{\equiv 0 \text{ for ART}}$	$\mathcal{L}_{YM} = \frac{1}{4} F_{\mu\nu a}{}^b\, F^{\mu\nu}{}_a{}^b$

QuantumCromoDynamic:

$(SU(3)_{(c)}$- Color Yang-Mills-Gauge Theory)

$$\boxed{\begin{array}{c} D_{\beta A}{}^B = \partial_\beta\, 1_A{}^B + ig\, G_{\beta A}{}^B \\ {}_A,{}^B = \text{red, green, blue} \end{array}}$$

$$\psi^f_A = \begin{pmatrix} \psi^f_r \\ \psi^f_g \\ \psi^f_b \end{pmatrix}$$

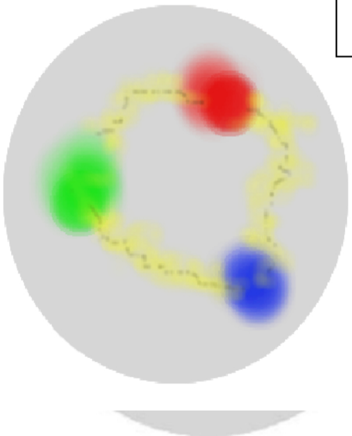

Confinement

chiral symmetry, ...

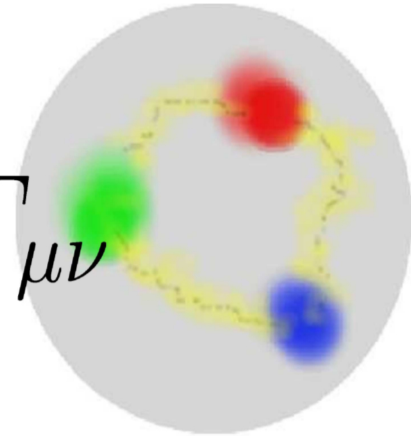

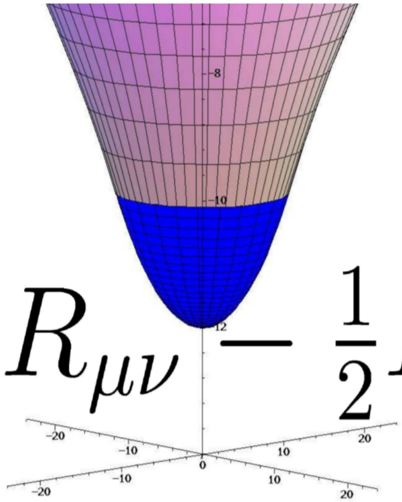

$$R_{\mu\nu} - \frac{1}{2} R\, g_{\mu\nu} = \frac{8\pi G}{c^4}\, T_{\mu\nu}$$

The Equation of State and the QCD Phase Diagram

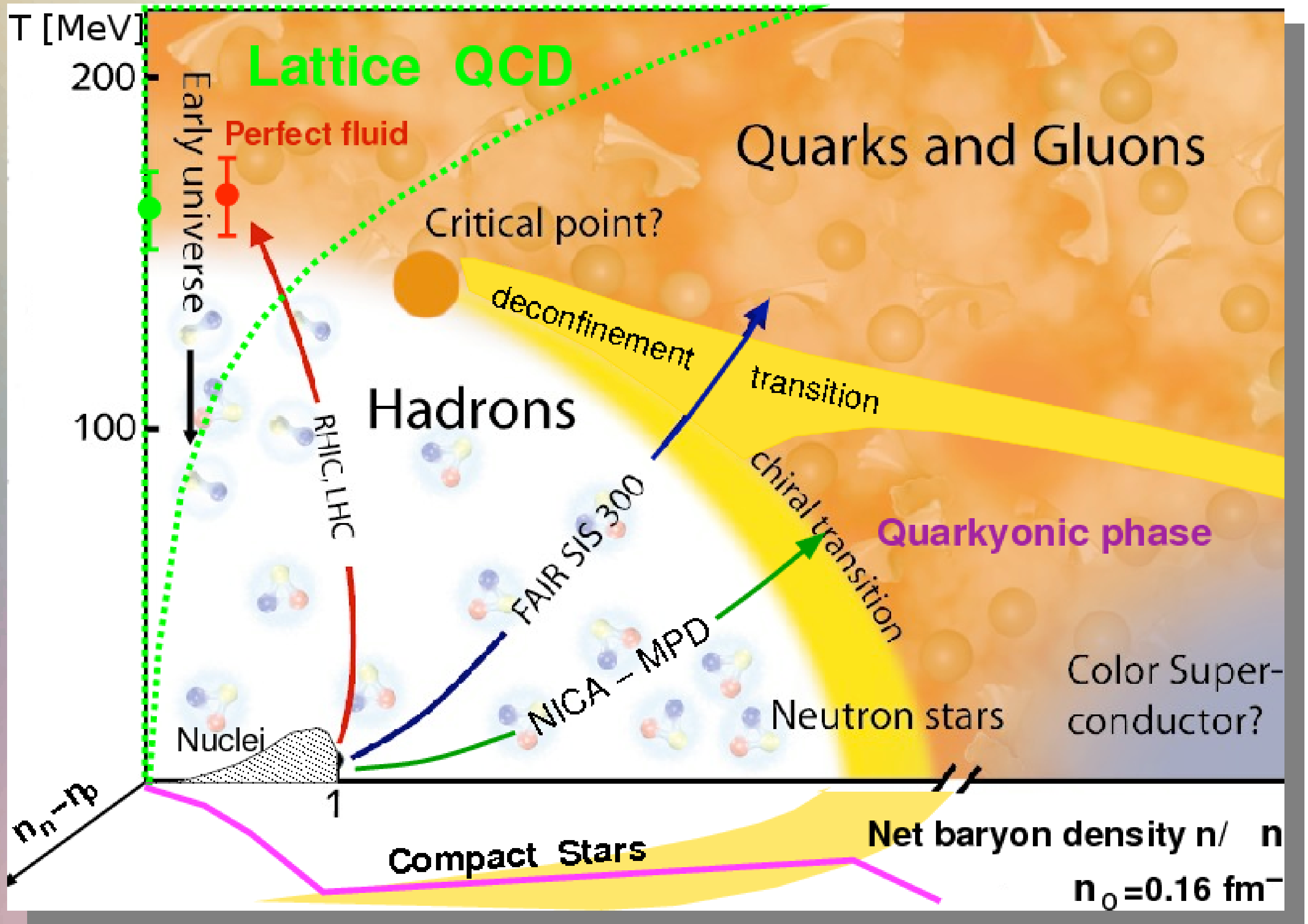

Image from http://inspirehep.net/record/823172/files/phd_qgp3D_quarkyonic2.png

The Gibbs Construction

Hadronic and quark matter surface:

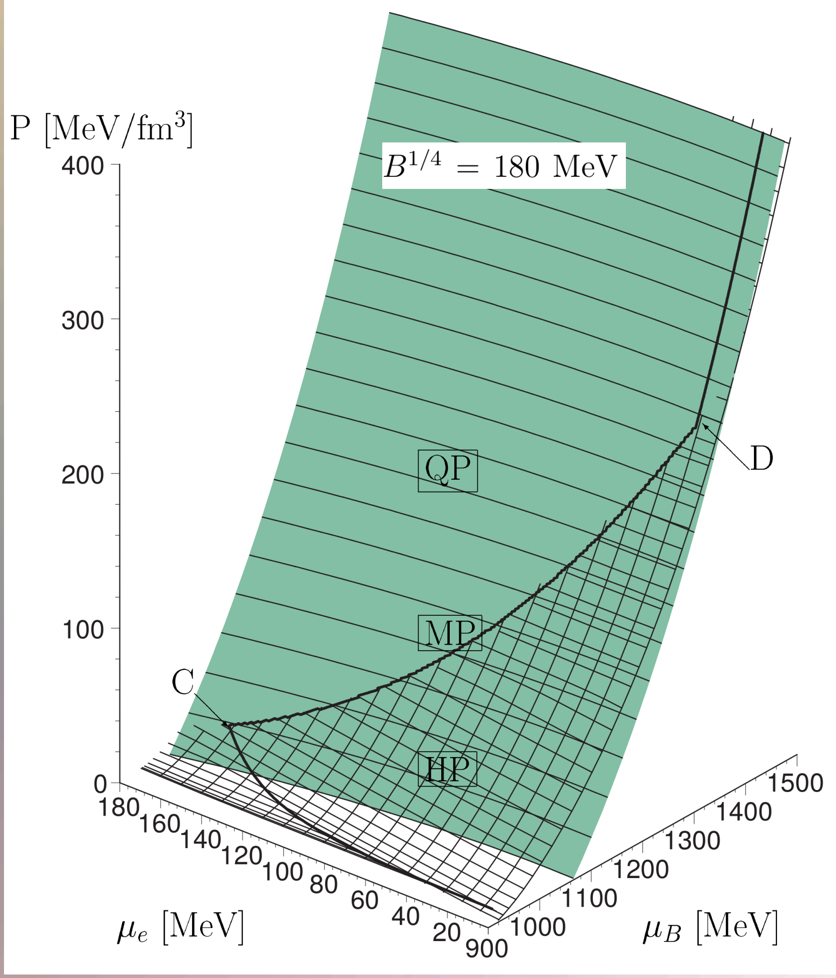

Charge neutrality condition is only globally realized

$$\rho_e := (1-\chi)\rho_e^H(\mu_B,\mu_e) + \chi\rho_e^Q(\mu_B,\mu_e) = 0\,.$$

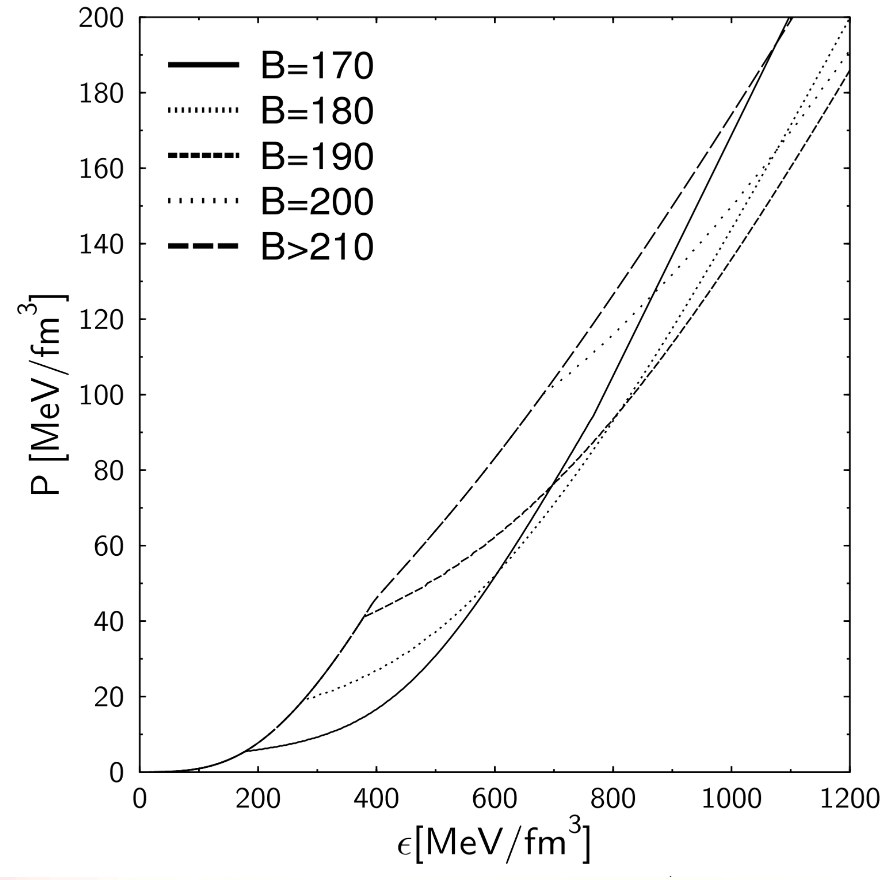

The QCD – Phase Transition and the Interior of a Hybrid Star

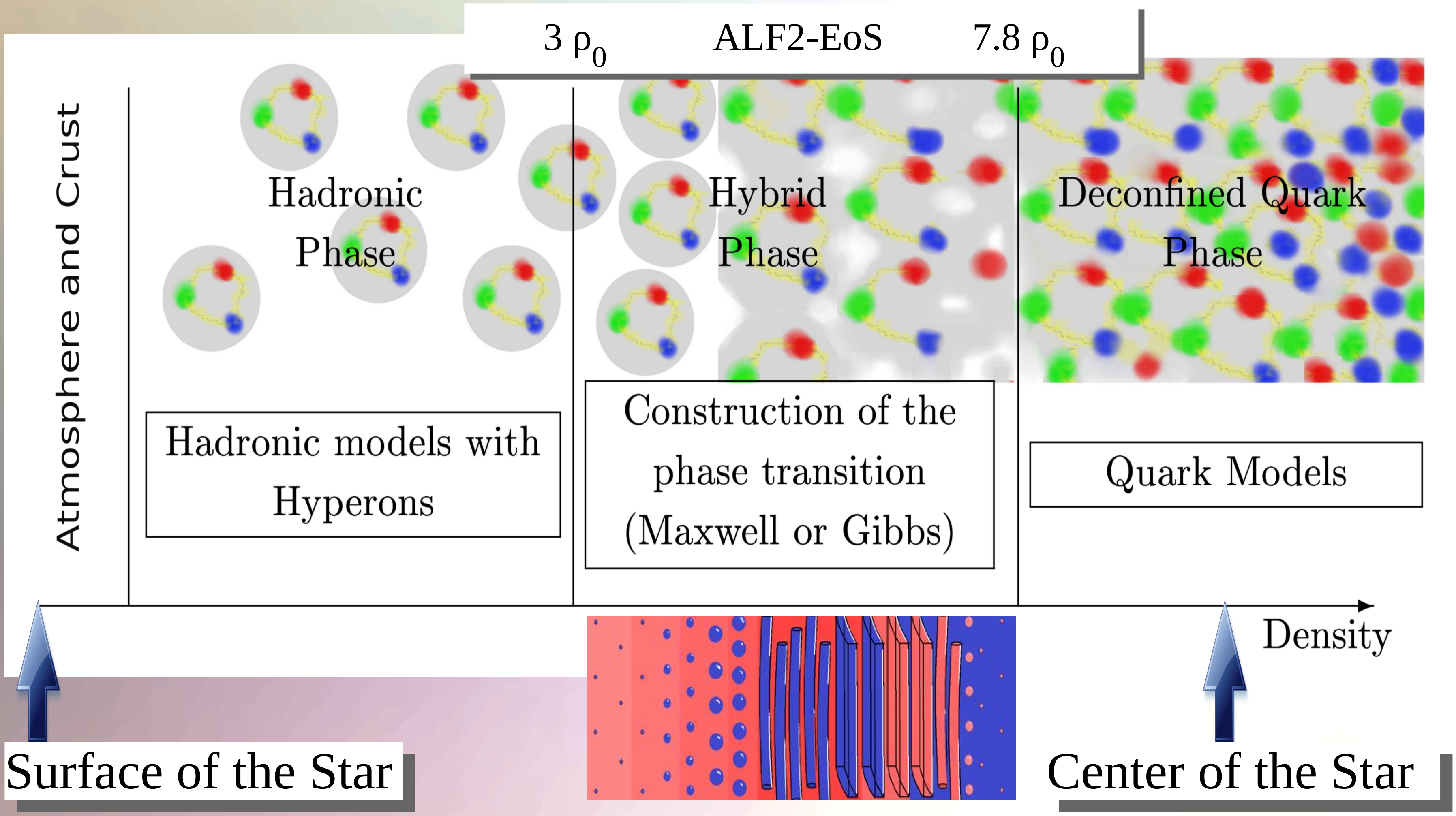

The Maxwell Construction

No Mixed Phase Region

Pressure and baryon chemical potential stays constant, while the density and the charge chemical potential jump discontinuously during the phase transition.

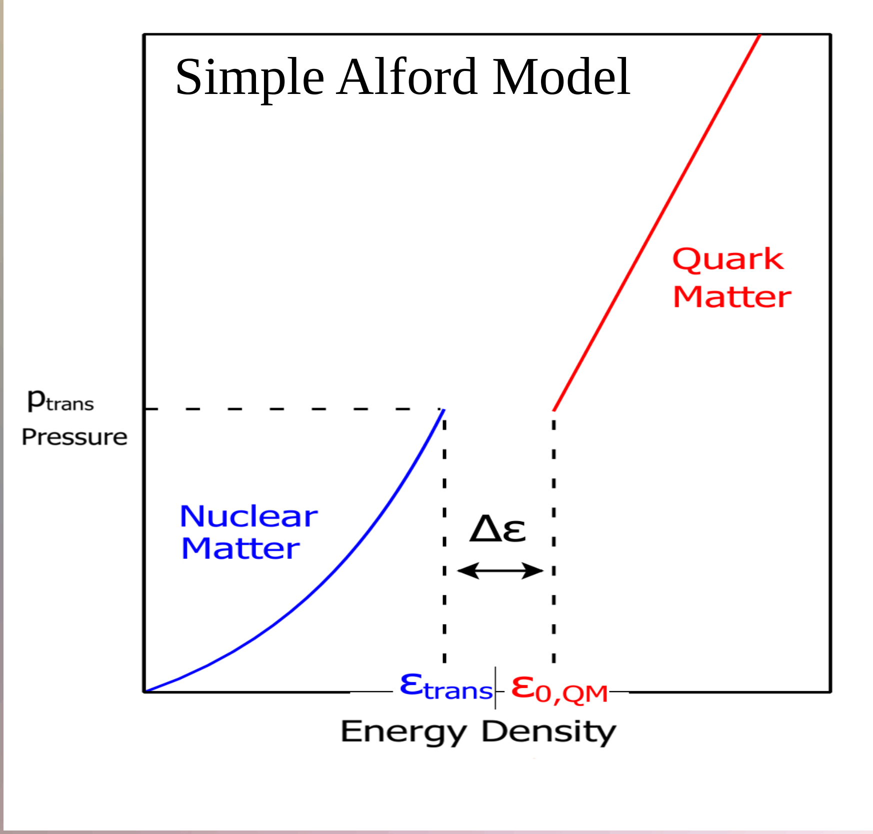

Hadronic Phase: DD2-Model
Quark Phase: Chiral Quark Meson Model

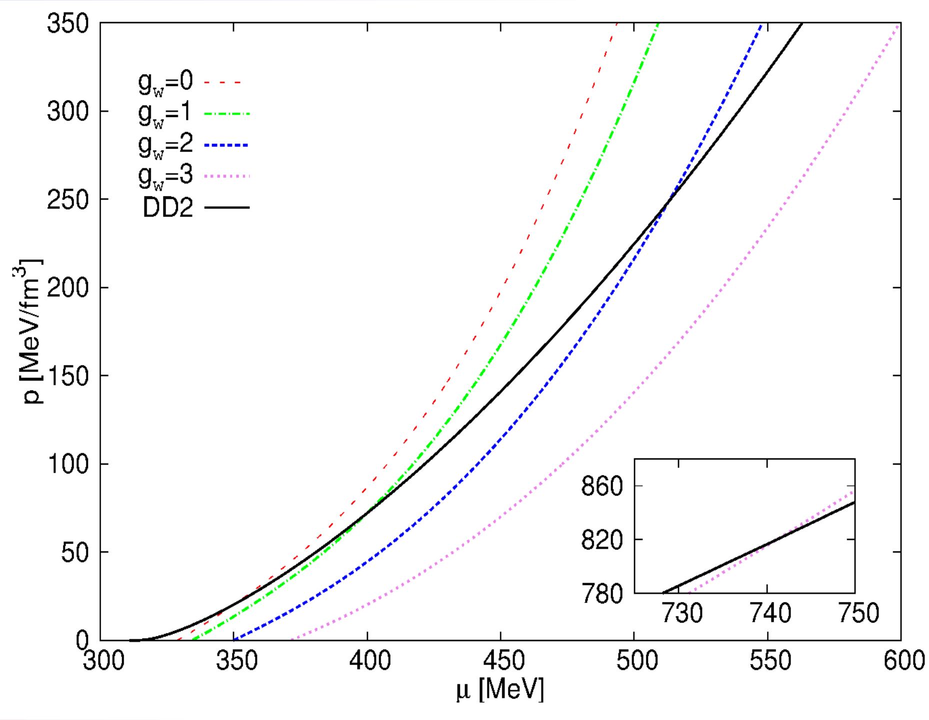

Image from M.G. Alford, S. Han, and M. Prakash, Phys. Rev. D 88, 083013 (2013)

A.Zacchi, M.Hanauske and Schaffner-Bielich, Phys. Rev. D 93, 065011 (2016)

The Compact Star Zoo

Depending on the model used, the compact star zoo consists of different inhabitants: e.g. neutron stars with and without hyperons, quark stars and strange quark stars, hybrid stars with color superconducting quark matter, hybrid stars with Bose-Einstein condensates of antikaons.

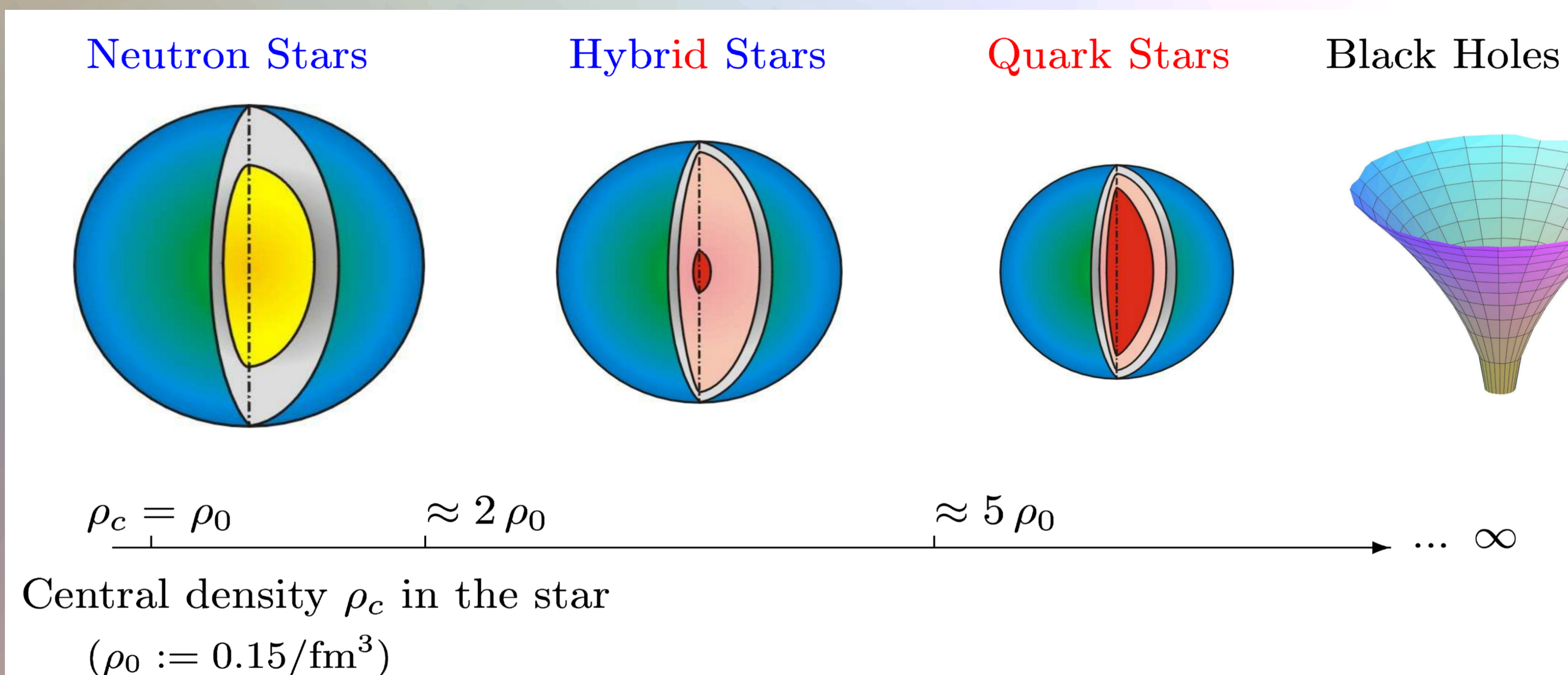

Numerical Setup

Several different EOSs : ALF2, APR4, GNH3, H4 and Sly, approximated by piecewise polytopes. Thermal ideal fluid component (Γ=2) added to the nuclear-physics EOSs.

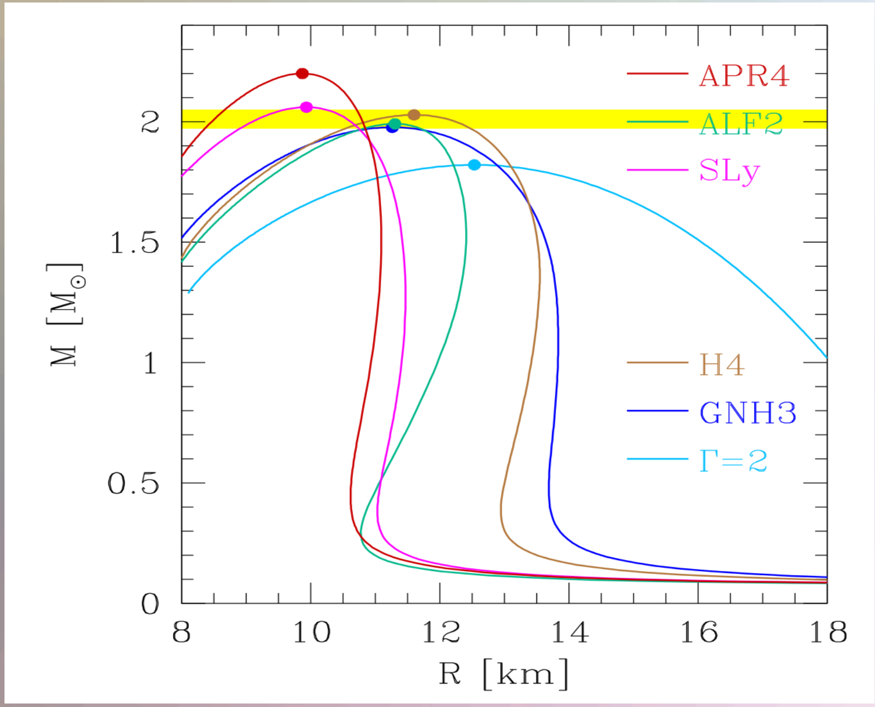

LS220: Temperature dependent
EOS-table (Lattimer-Swesty)

BSSNOK conformal traceless formulation of the ADM equations. 3+1 Valencia formulation and high resolution shock capturing methods for the hydrodynamic evolution. Full general relativity using the **Einstein-Toolkit** and the **WHISKY/WhiskyTHC code** for the general-relativistic hydrodynamic equations.

Grid Structure:

Adaptive mesh refinement (six ref. levels)

Grid resolution: (from 221 m to 7.1 km)

Outer Boundary: 759 km

Initial separation of stellar cores: 45 km

HMNS Evolution for different EoSs

High mass simulations (M=1.35)

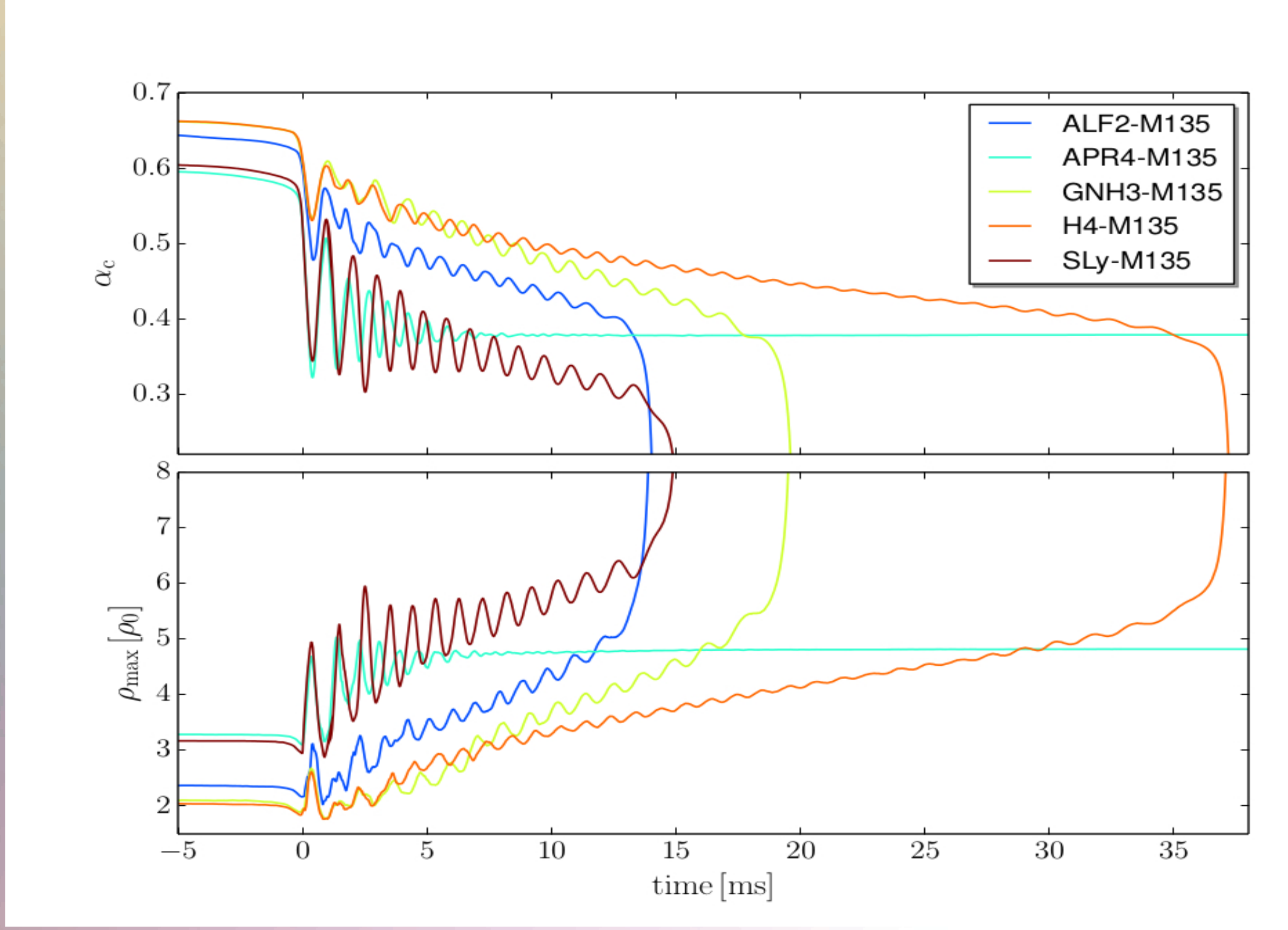

Central value of the lapse function α_c (upper panel) and maximum of the rest mass density ρ_{max} in units of ρ_0 (lower panel) versus time for the high mass simulations.

HMNS Evolution for different EoSs

Low mass simulations (M=1.25)

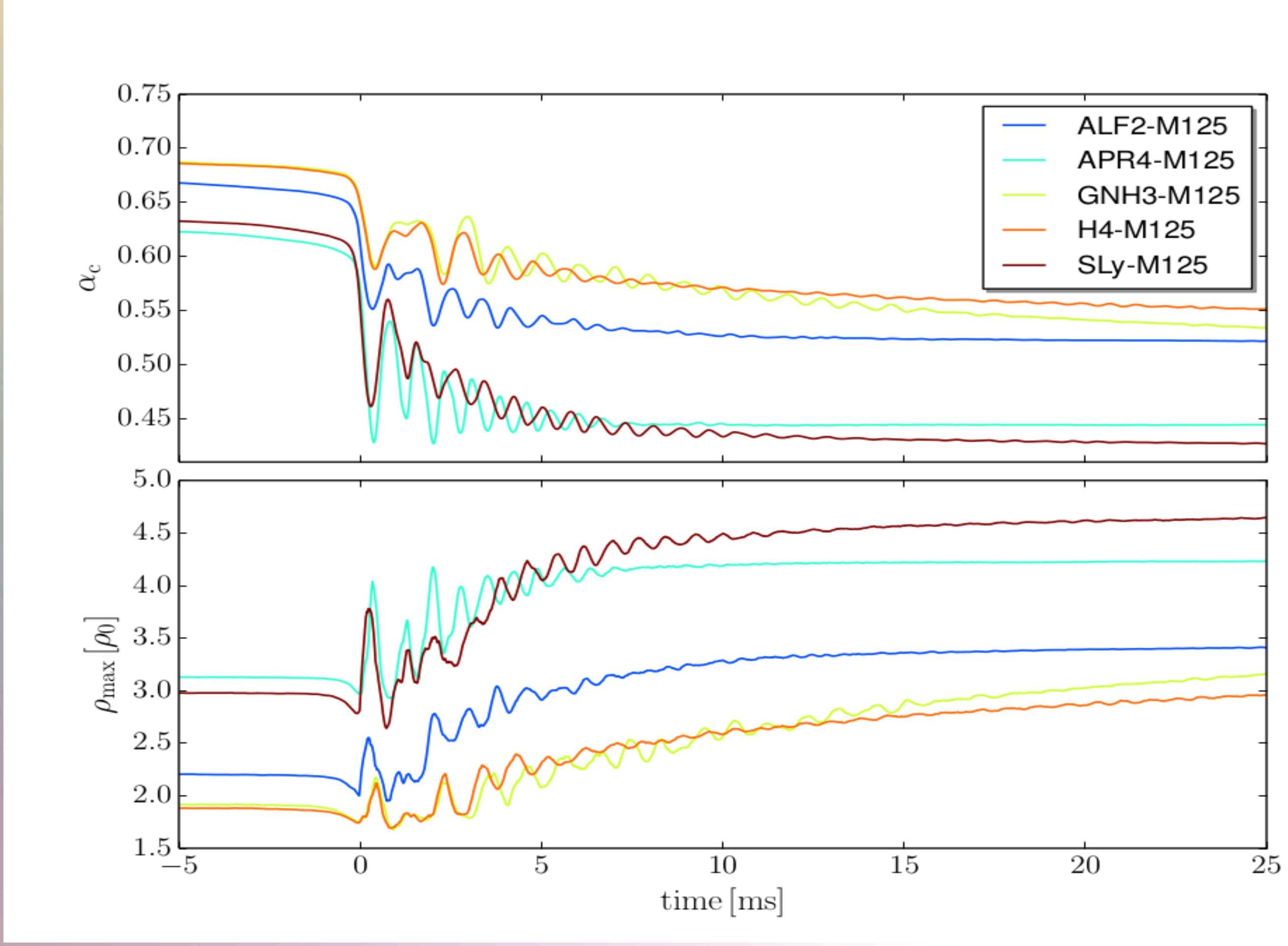

Central value of the lapse function α_c (upper panel) and maximum of the rest mass density ρ_{max} in units of ρ_0 (lower panel) versus time for the low mass simulations .

Evolution of the rest-mass density distribution

ALF2, High mass model: Mixed phase region starts at $3\rho_0$

Initial NS mass: 1.35 M_{solar}

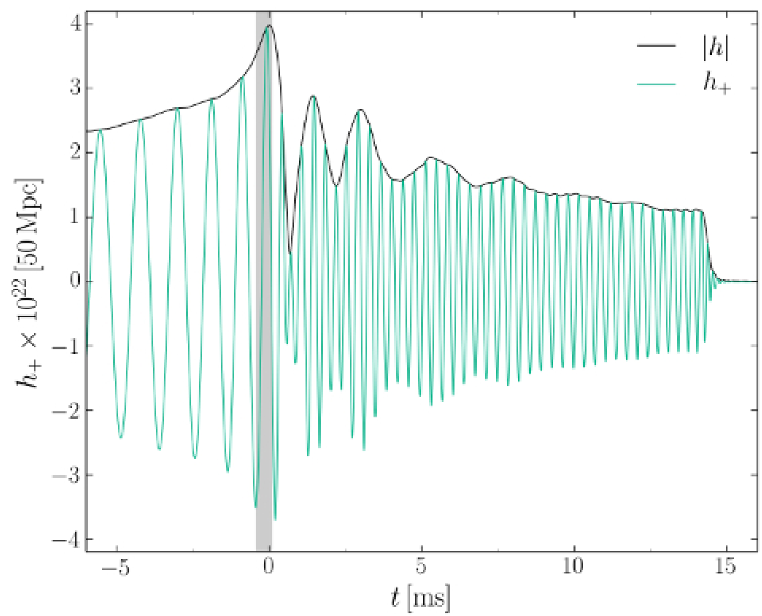

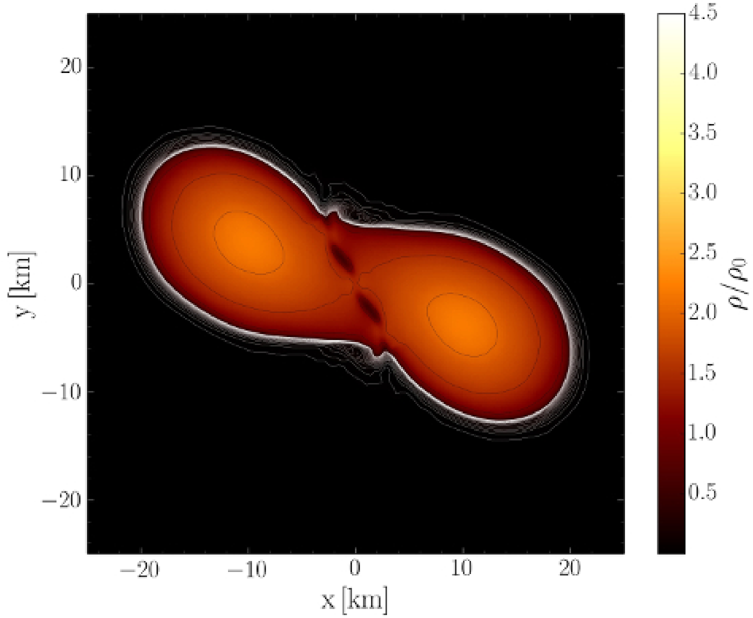

Gravitational wave amplitude at a distance of 50 Mpc

Rest mass density distribution $\rho(x,y)$ in the equatorial plane in units of the nuclear matter density ρ_0

The Angular Velocity in the (3+1)-Split

The angular velocity Ω in the (3+1)-Split is a combination of the lapse function α , the φ-component of the shift vector β^φ and the 3-velocity v^φ of the fluid (spatial projection of the 4-velocity **u**):

$$\boxed{\Omega(x, y, z, t) = \frac{u^\phi}{u^t} = \alpha\, v^\phi - \beta^\phi}$$

Angular velocity Ω

Lapse function α

Φ-component of 3-velocity v^φ

Frame-dragging β^φ

(3+1)-decomposition of spacetime:

$$g_{\mu\nu} = \begin{pmatrix} -\alpha^2 + \beta_i \beta^i & \beta_i \\ \beta_i & \gamma_{ij} \end{pmatrix}$$

Focus: Inner core of the differentially rotating HMNS

M. Shibata, K. Taniguchi, and K. Uryu, Phys. Rev. D 71, 084021 (2005)
M. Shibata and K. Taniguchi, Phys. Rev. D 73, 064027 (2006)
F. Galeazzi, S. Yoshida and Y. Eriguchi, A&A 541, p. A156 (2012)
W. Kastaun and F. Galeazzi, Phys. Rev. D 91, p. 064027 (2015)

EoS: ALF2, M=1.35 Post-Merger Phase

Gravitational wave amplitude h_+ and |h| at a distance of 738 km

for the ALF2-M135 model

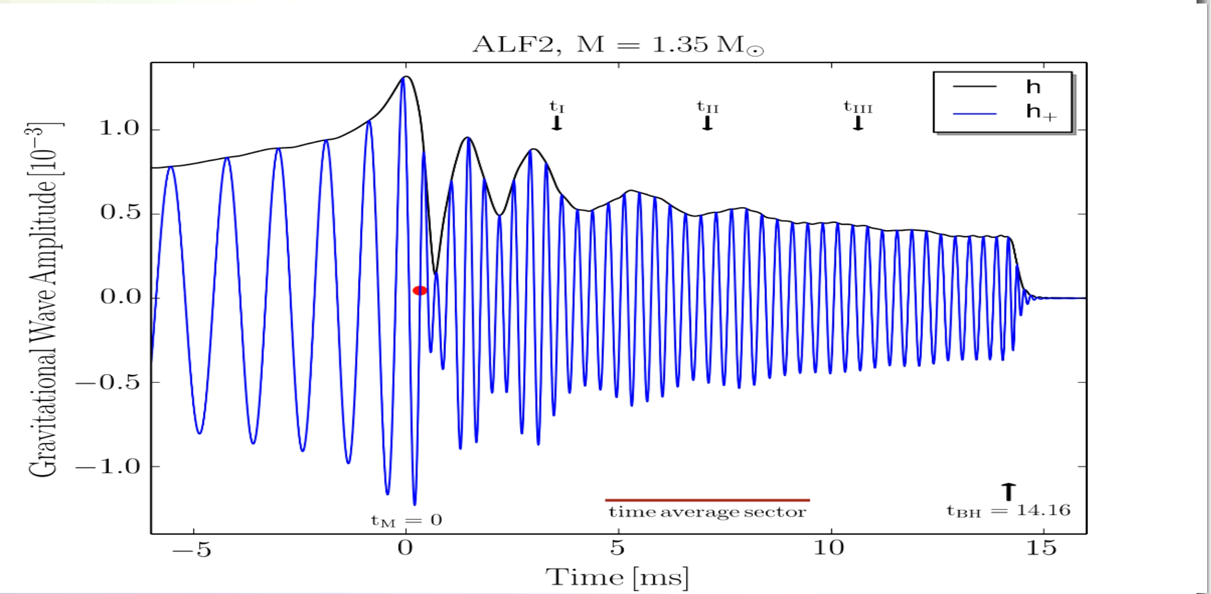

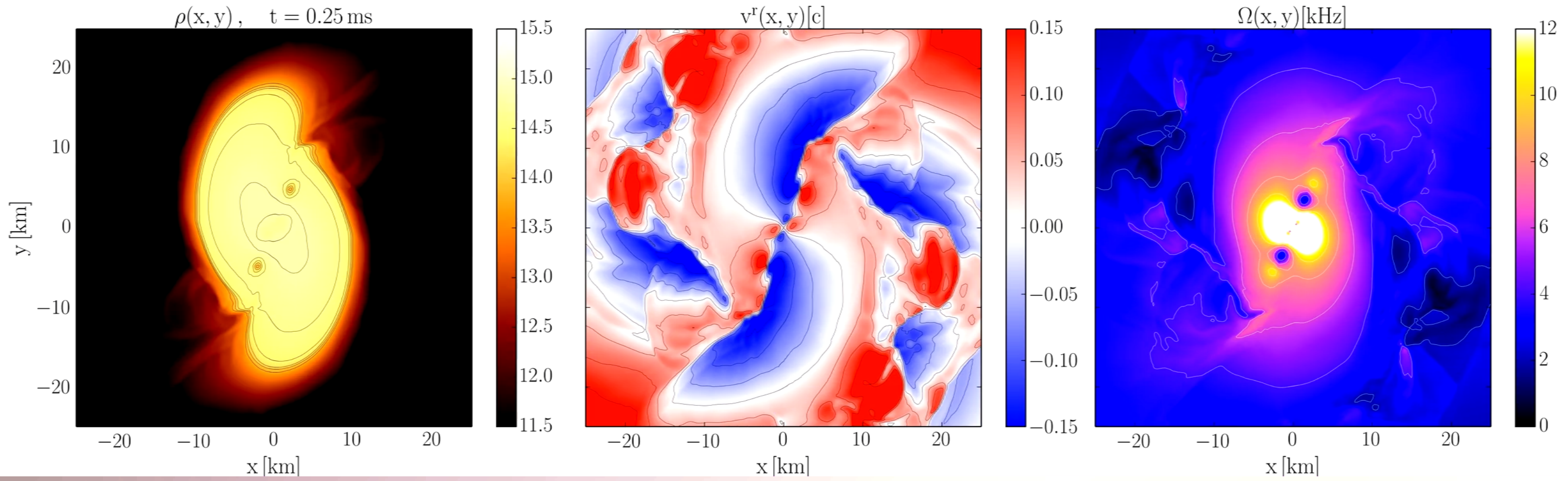

Rotation Profiles (ALF2-1.35 Model)

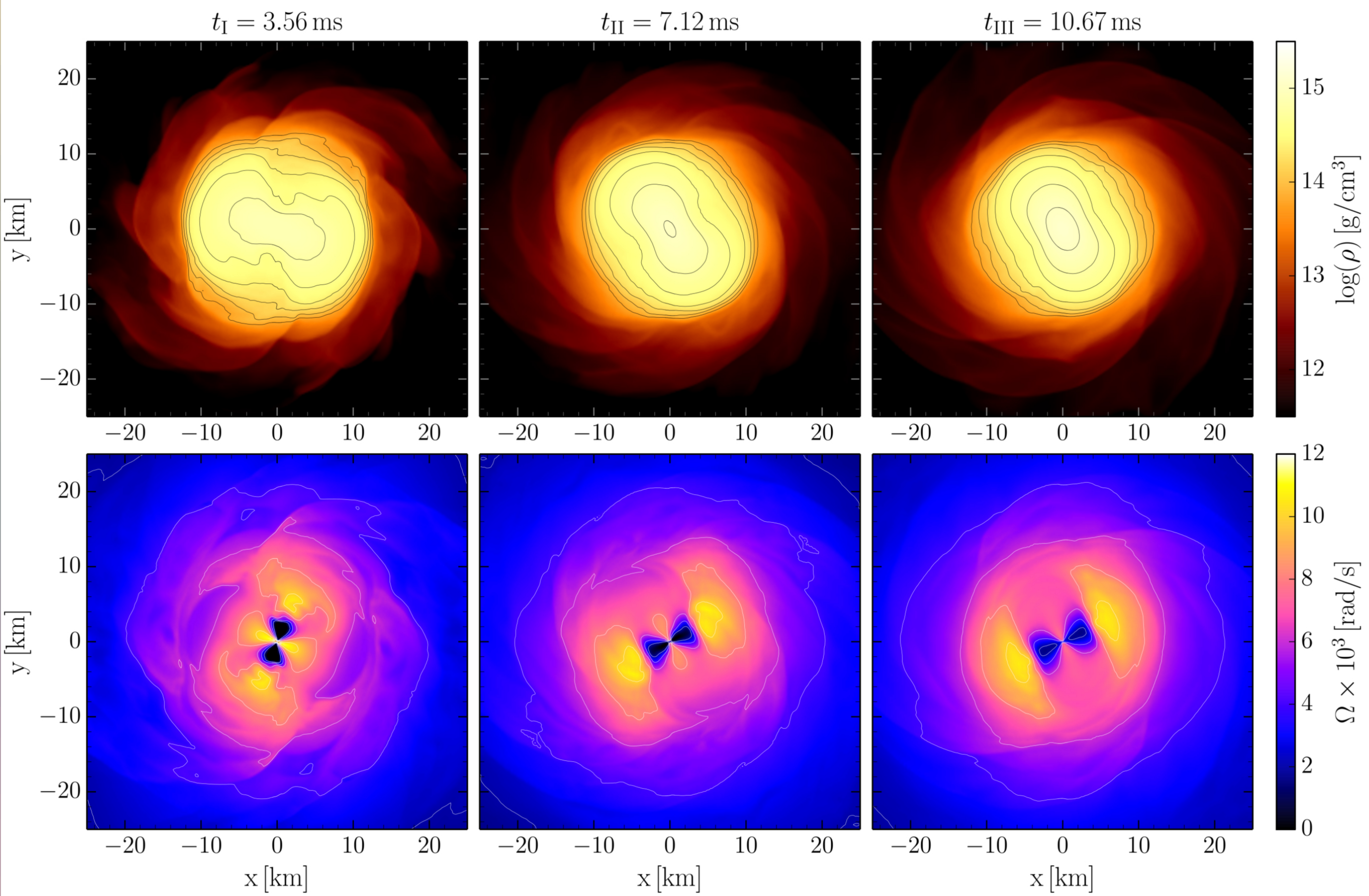

FIG. 3. Logarithm of the rest mass density Log(ρ) [g/cm^3] (upper row) and fluid angular velocity $\Omega \times 10^3$[rad/s] (lower row) in the xy-plane for the ALF2-M135 model at three different post-merger times. The iso-contour curves have been drawn at $13.8 + 0.2n$ (upper row) and $2n$ (lower row), $n \in \mathbb{N}$.

Rotation Profiles (ALF2-1.25 Model)

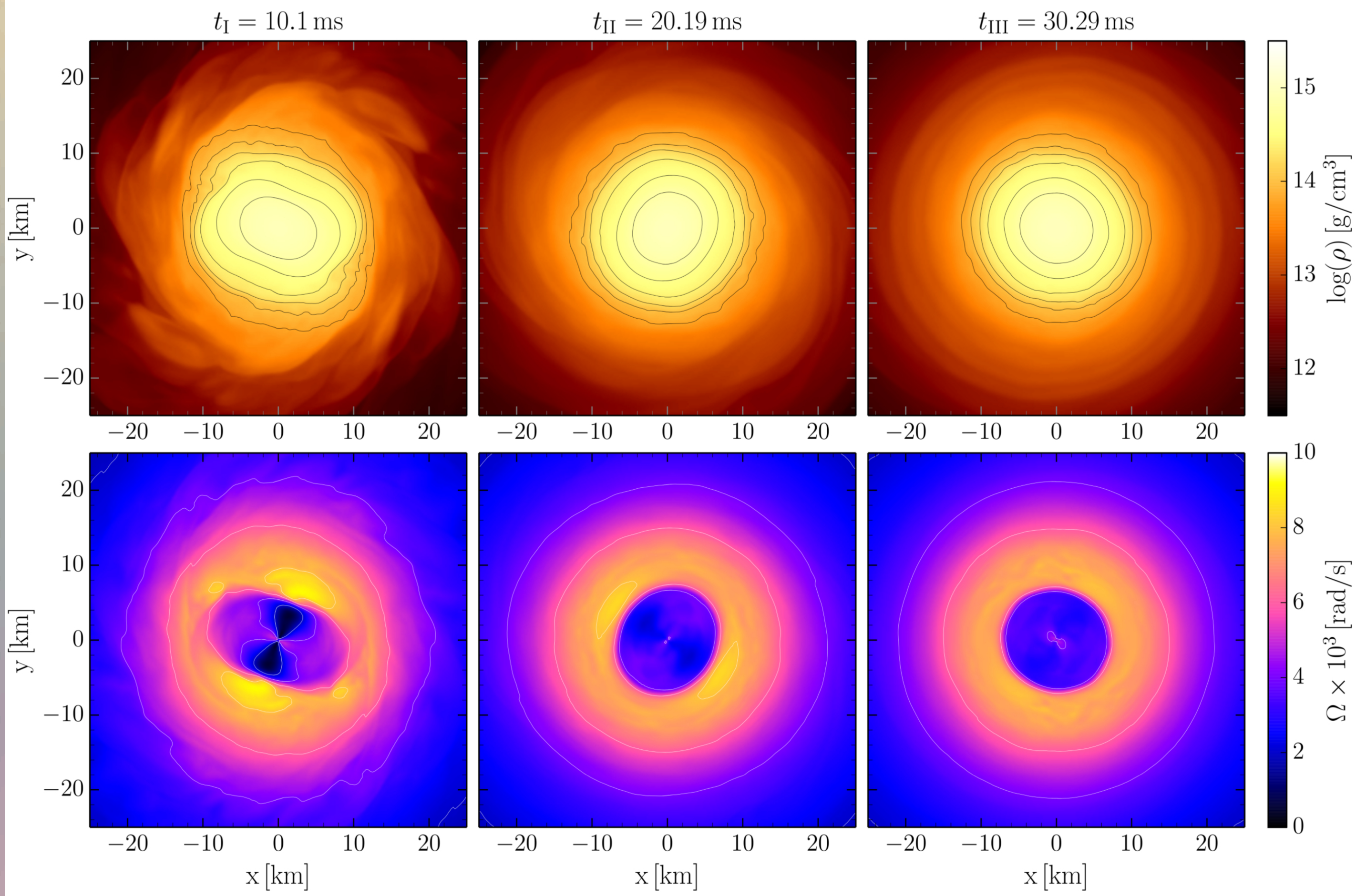

FIG. 11. Logarithm of the rest mass density Log(ρ) [g/cm^3] (upper row) and fluid angular velocity $\Omega \times 10^3$[rad/s] (lower row) in the xy-plane for the ALF2-M125 model at three different post-merger times. The iso-contour curves have been drawn at $13.8 + 0.2n$ (upper row) and $2n$ (lower row), $n \in \mathbb{N}$

LS220 M=1.32

Rest mass density, rotationprofile, Shift vector and Temperature

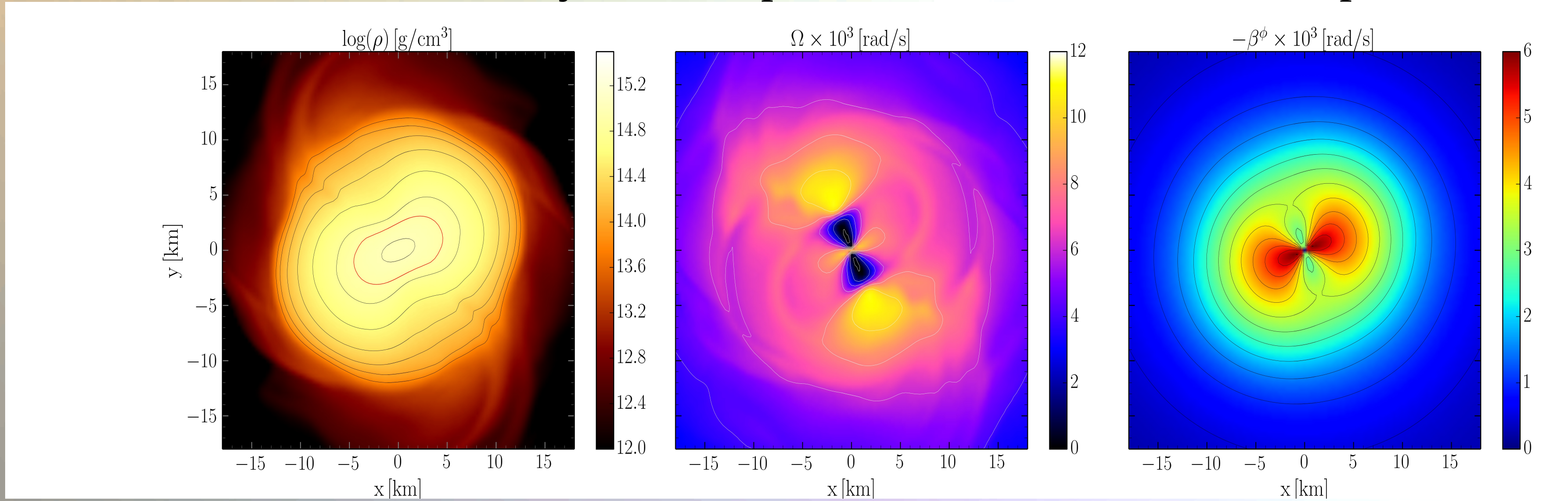

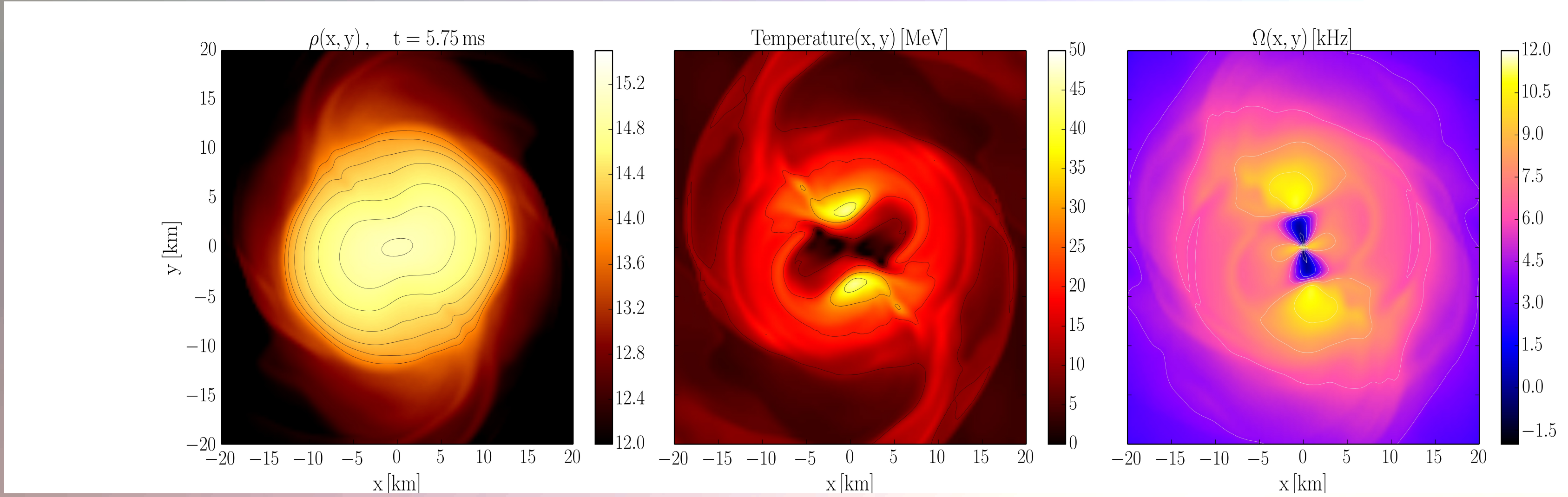

LS220 M=1.32

Co-rotating frame and fluid tracers

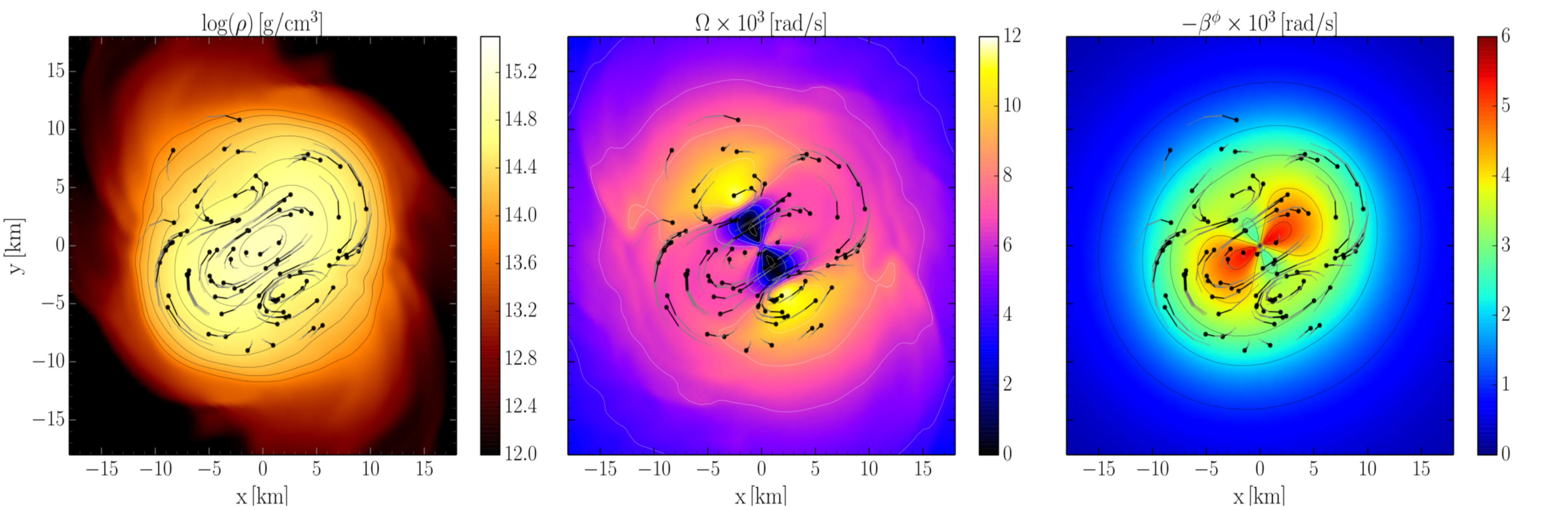

FIG. 7. Logarithm of the rest mass density Log(ρ) [g/cm^3] (left picture), the fluid angular velocity $\Omega \times 10^3$[rad/s] (middle) and $-\beta^\phi \times 10^3$[rad/s] (right picture) in the xy-plane for the SLY-M132 model at $t = 6.71$ ms. The trajectories of several tracer-cells are additionally mapped for two previous times (separation Δt_{Tr} =0.095 ms).

LS220 M=1.32

Co-rotating frame and fluid tracers

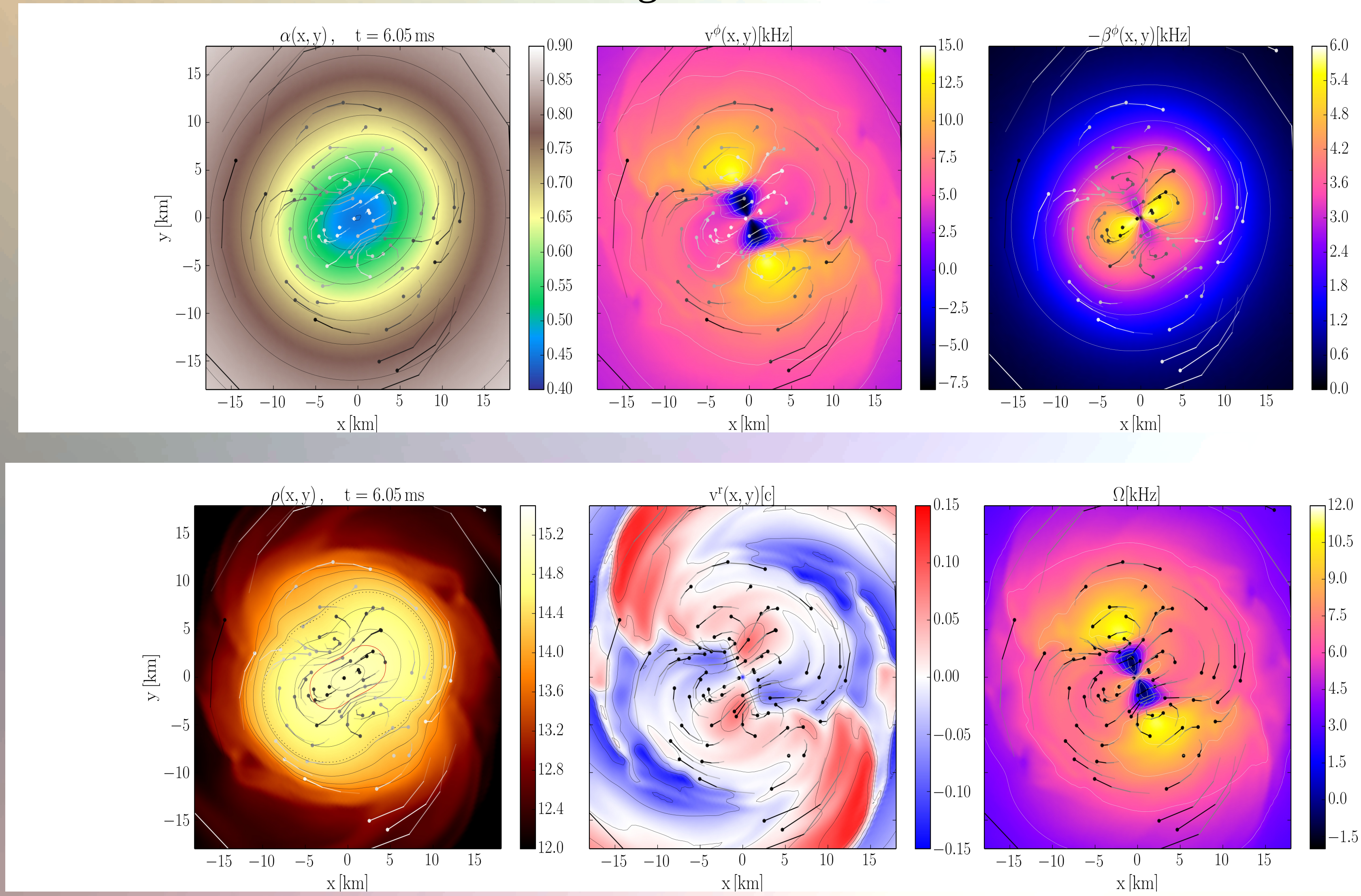

Temperature profiles in the (x,y)-plane

LS220-M132 binary at t = 6.7 ms (left panel) and t = 23.8 ms (right panel). The trajectories of several tracer-cells are additionally visualized.

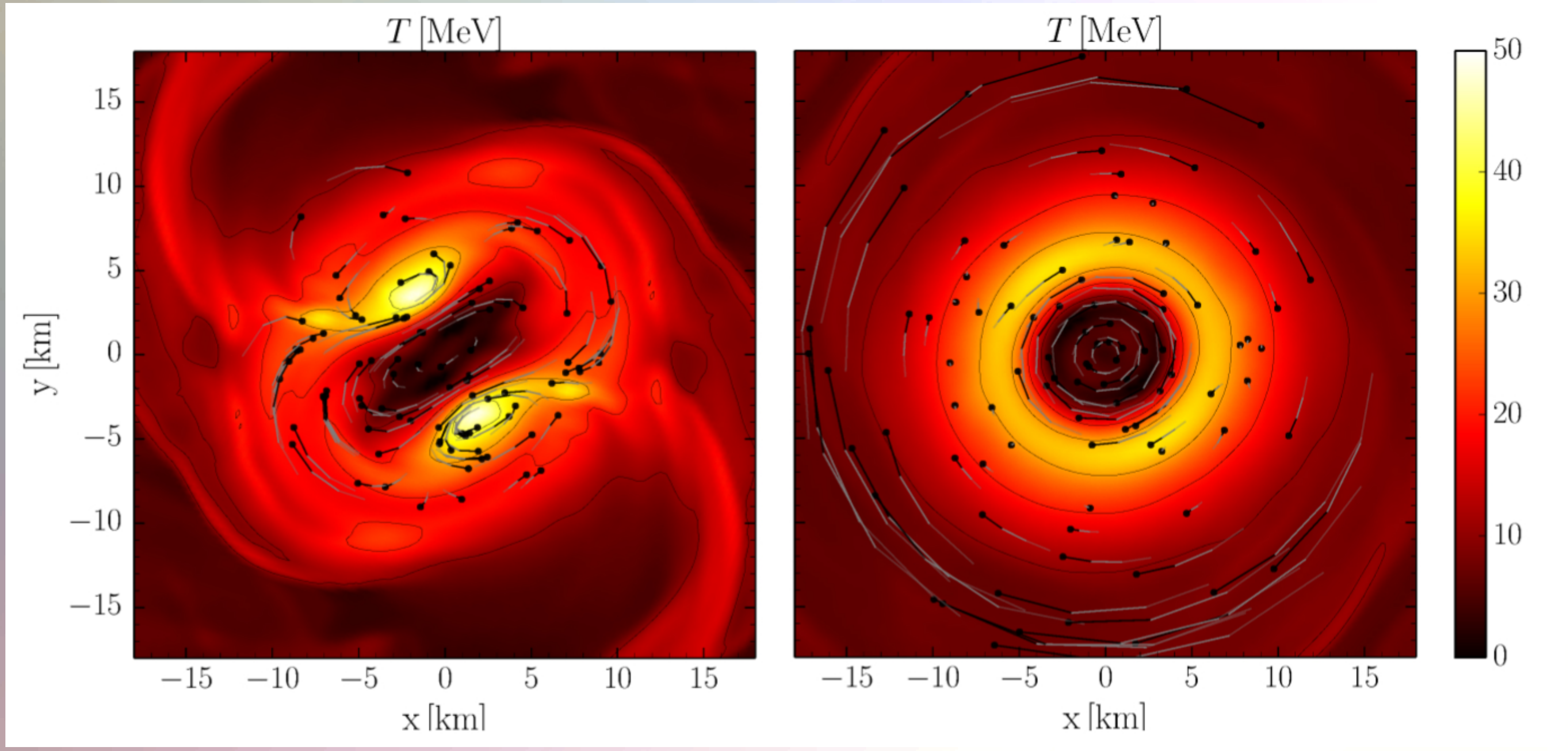

LS220 M=1.32

Co-rotating frame and fluid tracers

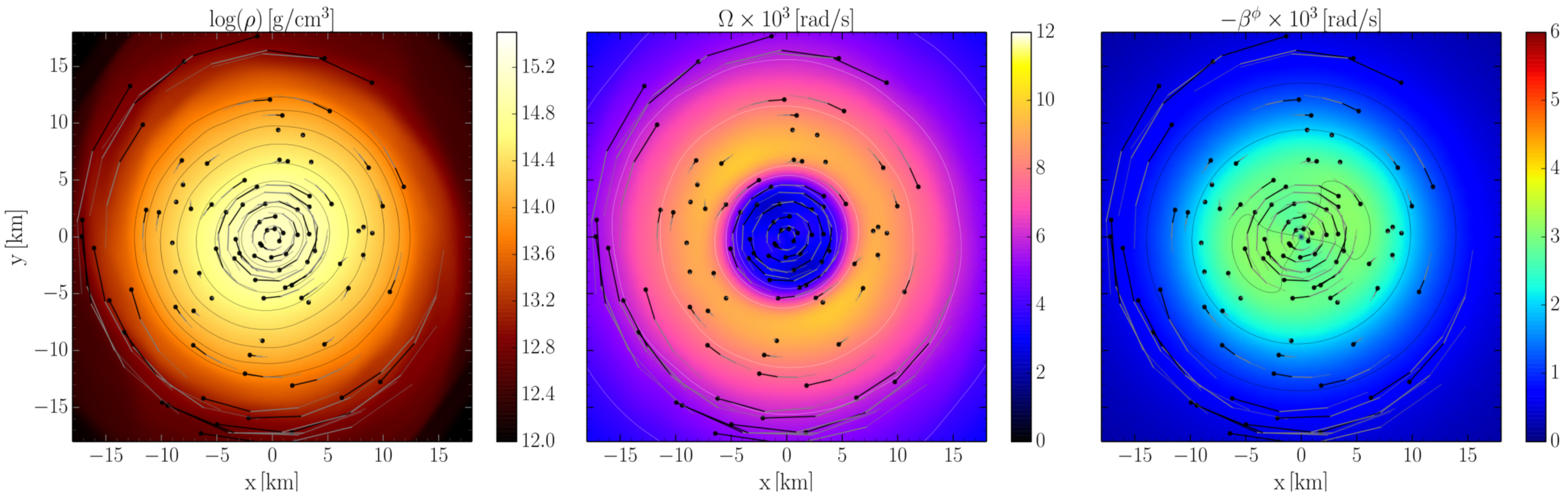

FIG. 8. Same as in Fig. 7, but at $t = 23.83$ ms.

LS220 M=1.32

Co-rotating frame and fluid tracers

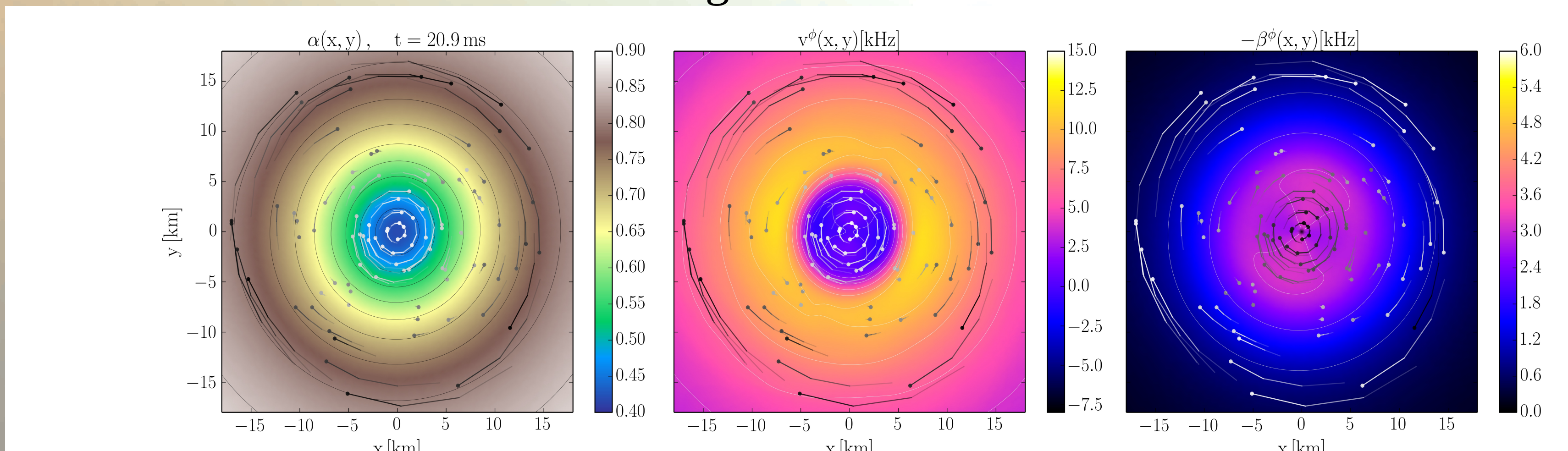

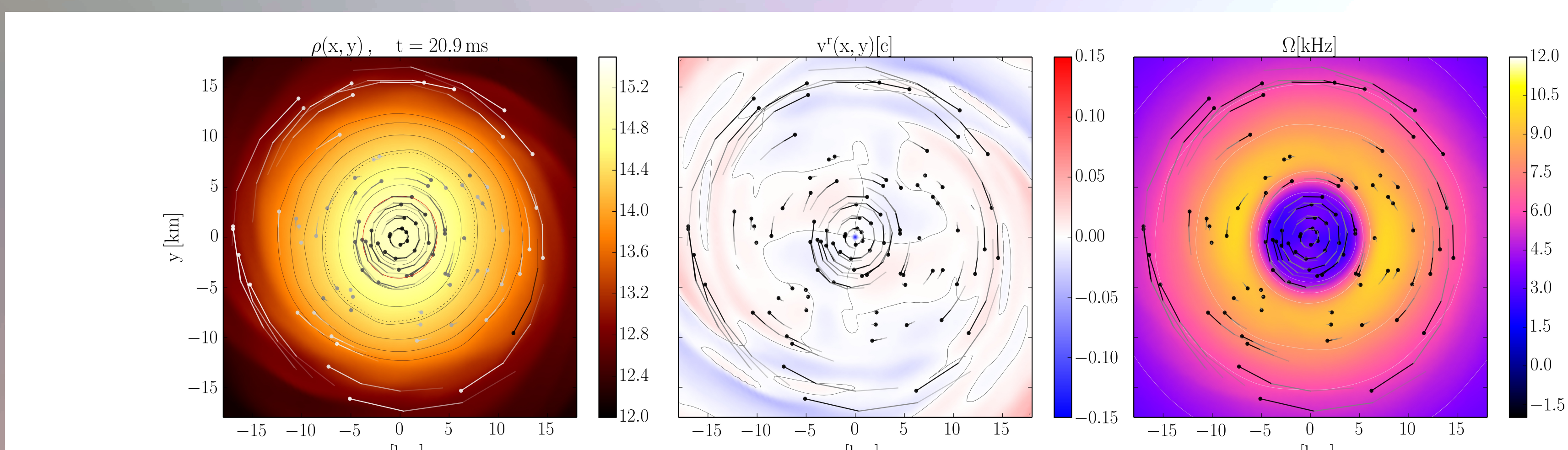

Averaging Procedure for Ω

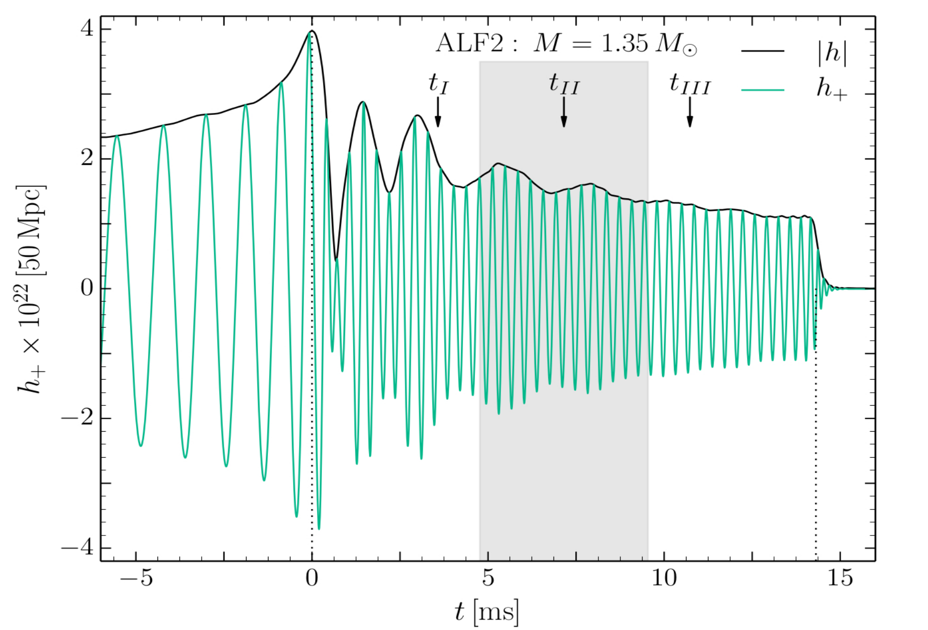

FIG. 2. Gravitational wave amplitude $|h|$ and h_+ at a distance of 50 Mpc for the ALF2-M135 model.

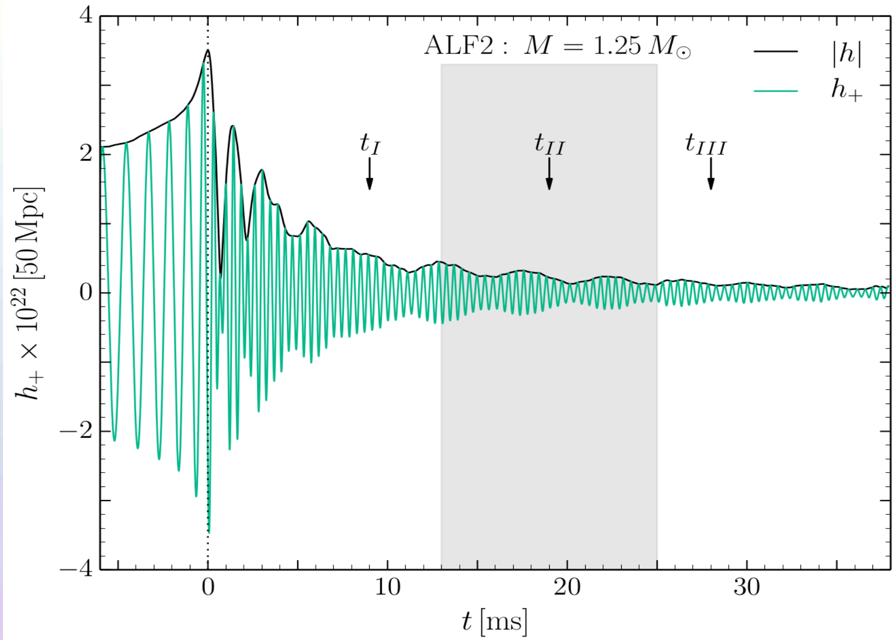

FIG. 10. Gravitational wave amplitude h_+ and $|h|$ at a distance of 50 Mpc for the ALF2-M125 model.

In order to compare the structure of the rotation profiles between the different EOSs, a certain time averaging procedure has been used:

$$\bar{\Omega}(r, t_c) = \int_{t_c-\Delta t/2}^{t_c+\Delta t/2} \int_{-\pi}^{\pi} \Omega(r, \phi, t')\; d\phi\, dt'$$

Time-averaged Rotation Profiles

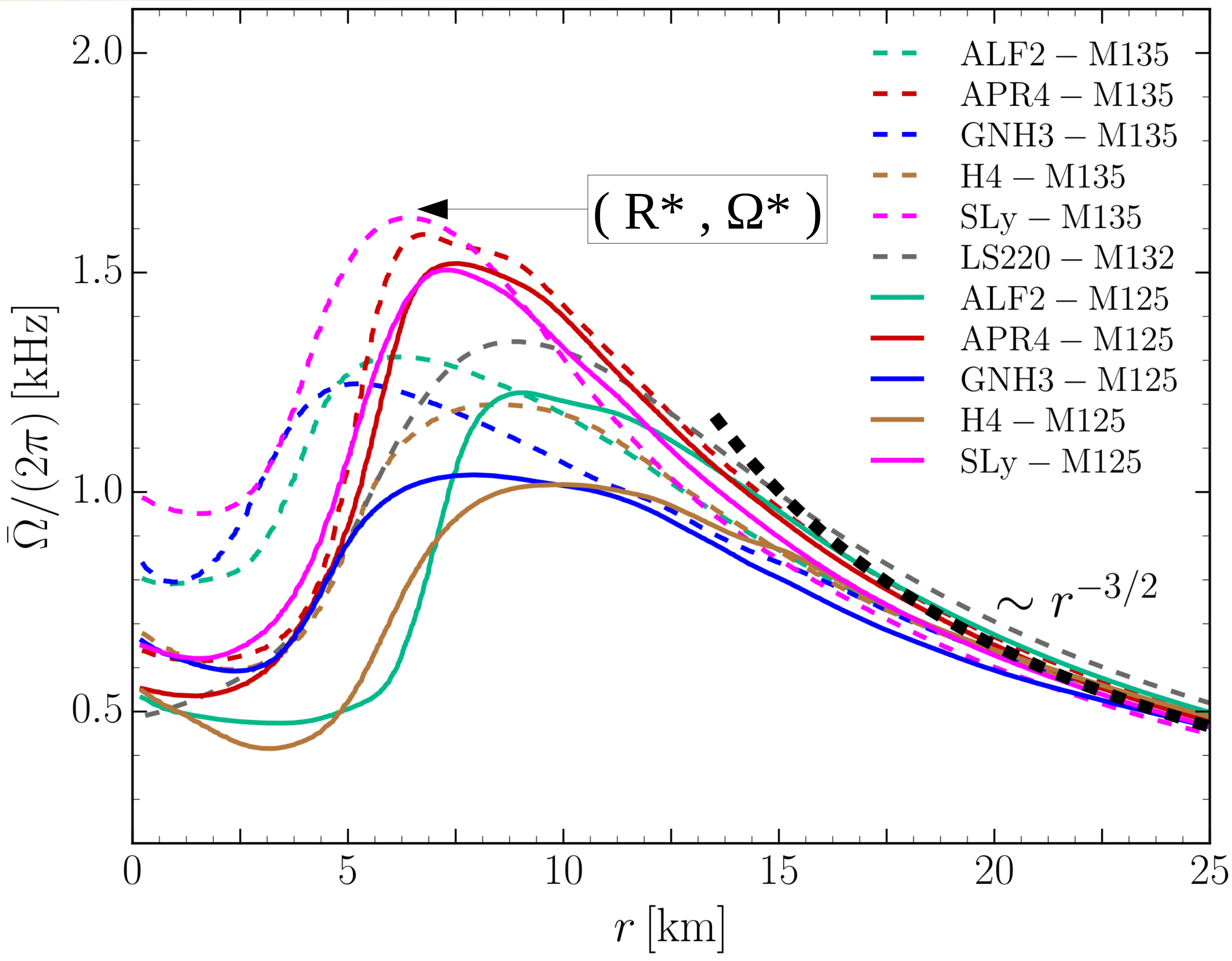

Soft EoSs:
Sly
APR4

Stiff EoSs:
GNH3
H4

Time-averaged rotation profiles for different EoS
Low mass runs (solid curves), high mass runs (dashed curves).

GW-Spectrum for different EoSs

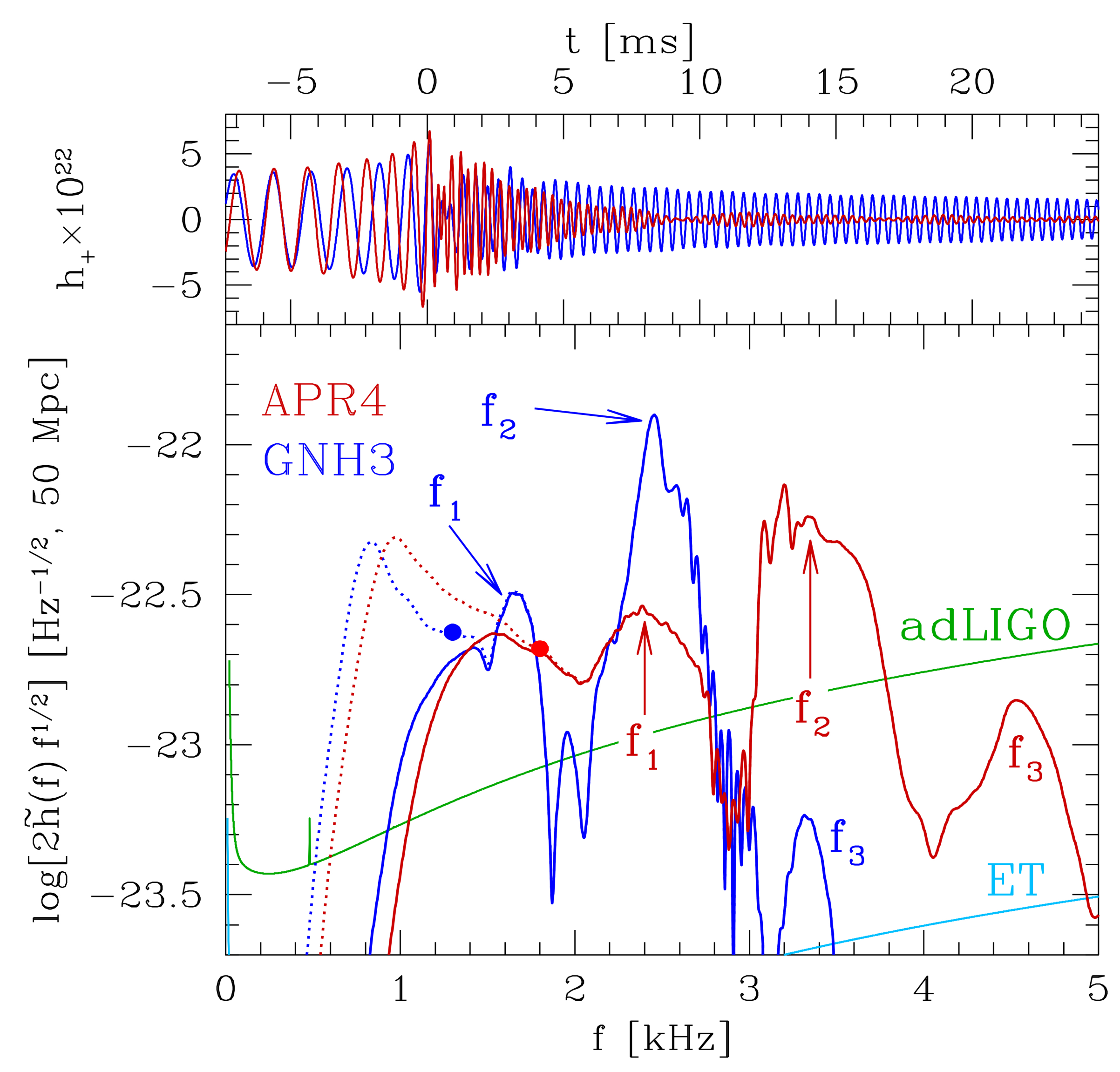

See:

Kentaro Takami, Luciano Rezzolla, and Luca Baiotti, Physical Review D 91, 064001 (2015)

Hotokezaka, K., Kiuchi, K., Kyutoku, K., Muranushi, T., Sekiguchi, Y. I., Shibata, M., & Taniguchi, K. (2013). Physical Review D, 88(4), 044026.

Bauswein, A., & Janka, H. T. (2012). Physical review letters, 108(1), 011101.

Clark, J. A., Bauswein, A., Stergioulas, N., & Shoemaker, D. (2015). arXiv:1509.08522.

Bernuzzi, S., Dietrich, T., & Nagar, A. (2015). Physical review letters, 115(9), 091101.

Time Evolution of the GW-Spectrum

The power spectral density profile of the post-merger emission is characterized by several distinct frequencies f_{max}, f_1, f_2, f_3 and f_{2-0}. After approximately 5 ms after merger, the only remaining dominant frequency is the f_2-frequency.

See L.Rezzolla and K.Takami, arXiv:1604.00246

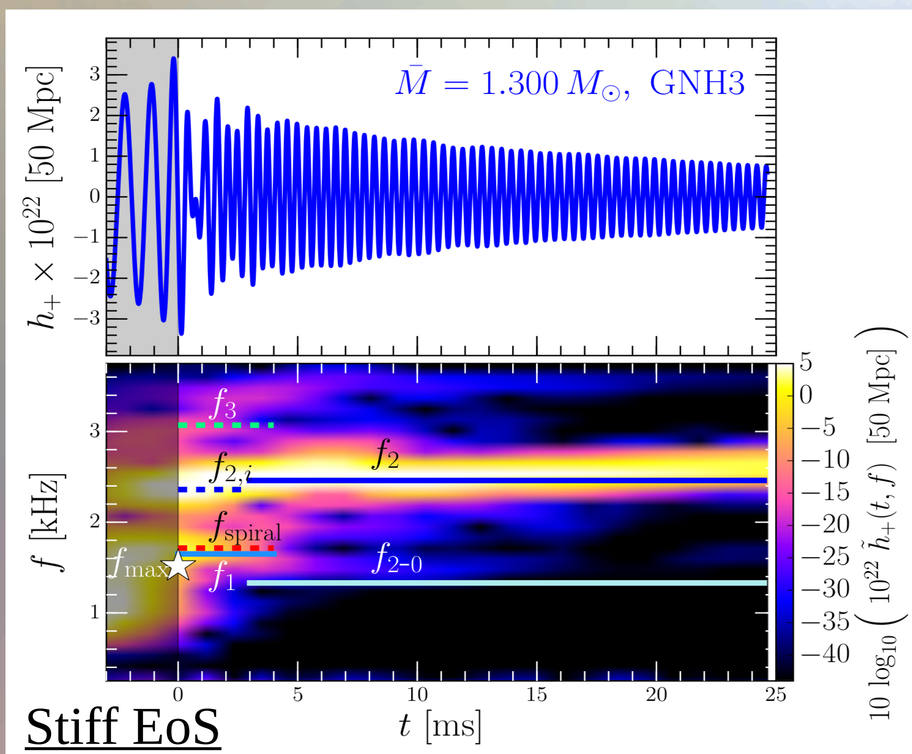

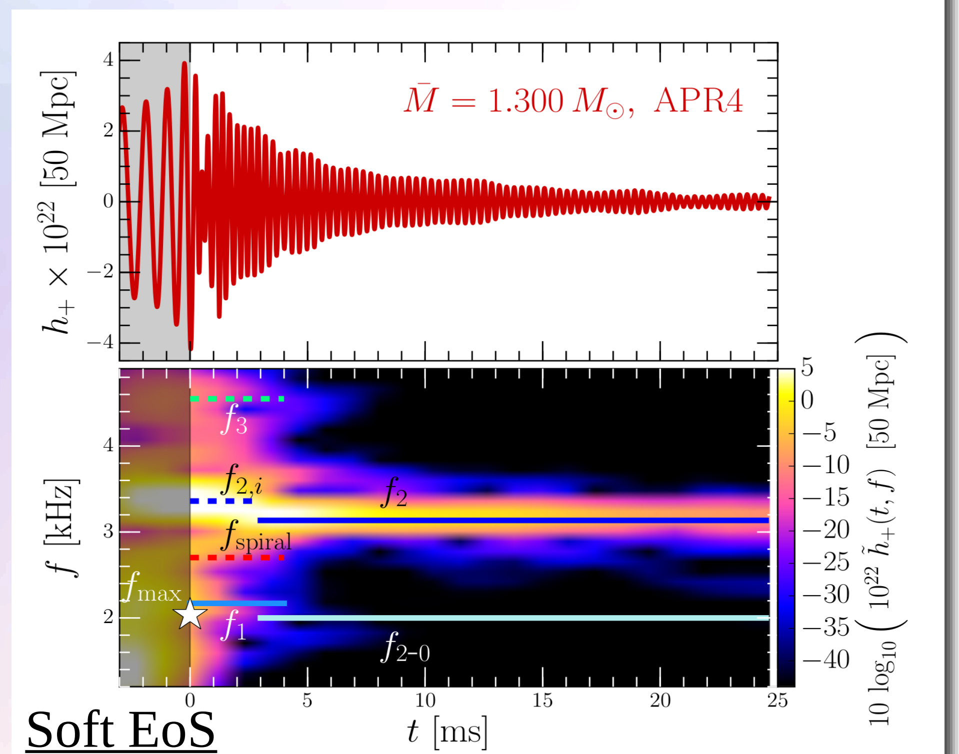

Evolution of the frequency spectrum of the emitted gravitational waves for the stiff GNH3 (left) and soft APR4 (right) EOS.

Gravitational Waves and the maximum of the Rotation Curve

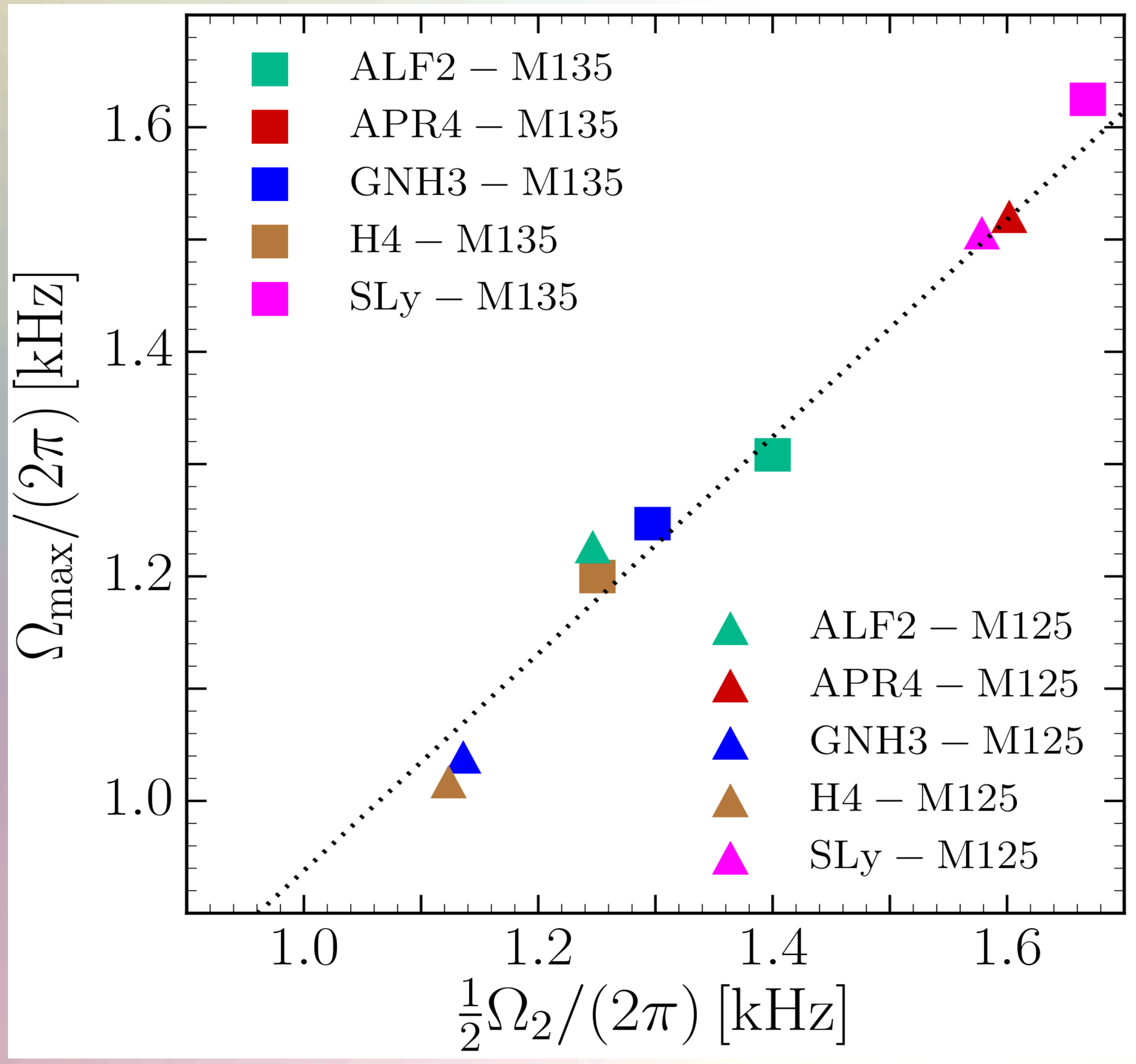

How to observe the QGP

with gravitational waves from NS mergers?

Outlook

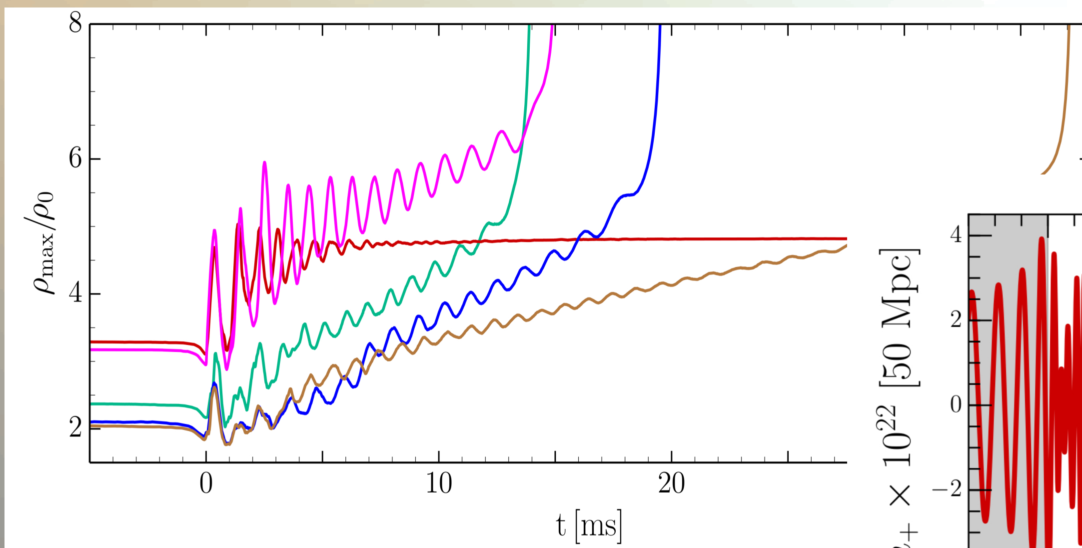

Maximum of the rest mass density ρ_{max}

in units of ρ_0 versus time

for the high mass simulations.

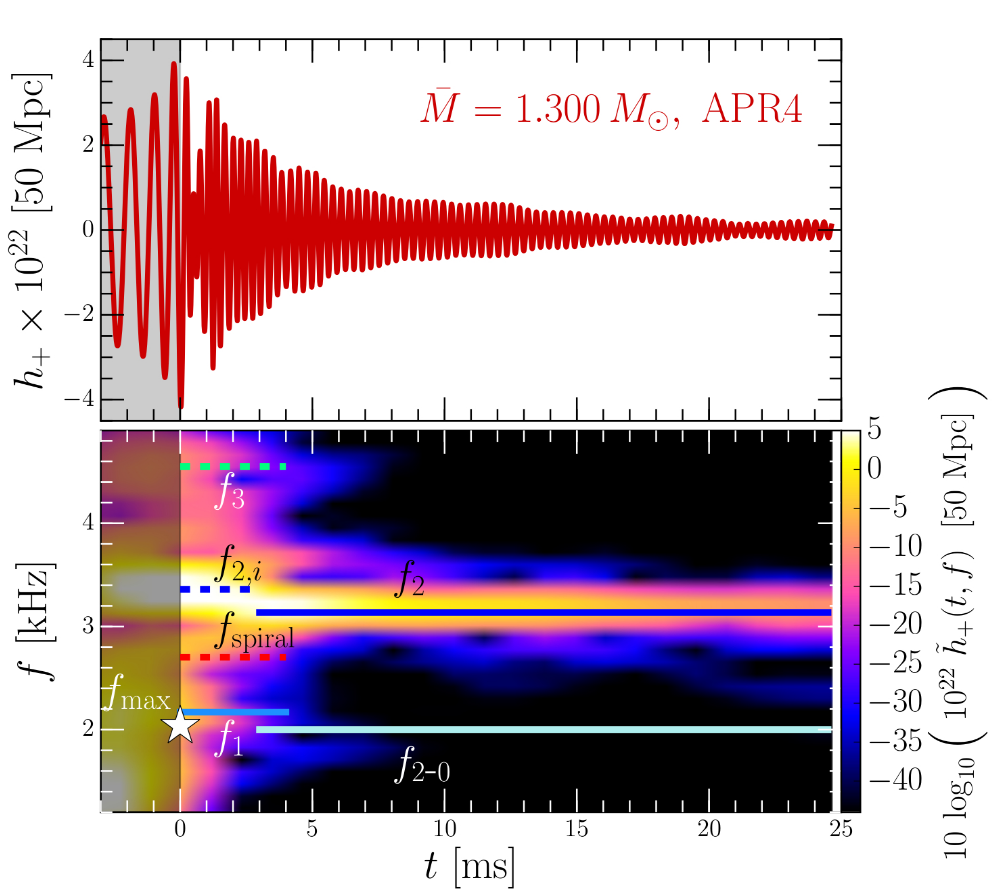

The power spectral density profile of the post-merger emission is characterized by several distinct frequencies f_{max}, f_1, f_2, …, $f_{2\text{-}PT}$

Summary

1. With the first observation of gravitational waves from binary black hole merger by LIGO, the whole branch of observational astronomy will enter a new era - the so called gravitational-wave astronomy.
2. GWs emitted from merging neutron star binaries are on the verge of their first detection.
3. The spectrum of the emitted GWs (within the merger and post-merger phase) depend strongly on the high density regime of the EOS.
4. With the knowledge of the f_1- and f_2-frequency peak and the total mass the system, the GW signal can set tight constraints on the EOS.
5. The phasetransition to the Quark-Gluon-Plasma might be observable with Gravitational Wave Detektors ($f_{2\text{-PT}}$ - peak)

Rotational properties of hypermassive neutron stars from binary mergers

Matthias Hanauske,[1,2] Kentaro Takami,[3,1] Luke Bovard,[1] Luciano Rezzolla,[1,2]
José A. Font,[4,5] Filippo Galeazzi,[1] and Horst Stöcker[1,2,6]

[1]*Institut für Theoretische Physik, Max-von-Laue-Straße 1, 60438 Frankfurt, Germany*
[2]*Frankfurt Institute for Advanced Studies, Ruth-Moufang-Straße 1, 60438 Frankfurt, Germany*
[3]*Kobe City College of Technology, 651-2194 Kobe, Japan*
[4]*Departamento de Astronomía y Astrofísica, Universitat de València, Dr. Moliner 50, 46100, Burjassot (València), Spain*
[5]*Observatori Astronòmic, Universitat de València, C/ Catedrático José Beltrán 2, 46980, Paterna (València), Spain*
[6]*GSI Helmholtzzentrum für Schwerionenforschung GmbH, D-64291 Darmstadt, Germany*

Determining the differential-rotation law of compact stellar objects produced in binary neutron stars mergers or core-collapse supernovae is an old problem in relativistic astrophysics. Addressing this problem is important because it impacts directly on the maximum mass these objects can attain and hence on the threshold to black-hole formation under realistic conditions. Using the results from a large number of numerical simulations in full general relativity of binary neutron star mergers described with various equations of state and masses, we study the rotational properties of the resulting hypermassive neutron stars. We find that the angular-velocity distribution shows only a modest dependence on the equation of state, thus exhibiting the traits of "quasi-universality" found in other aspects of compact stars, both isolated and in binary systems. The distributions are characterized by an almost uniformly rotating core and a quasi-Keplerian "disk". Such a configuration is significantly different from the $j - \mathrm{constant}$ differential-rotation law that is commonly adopted in equilibrium models of differentially rotating stars. Furthermore, the rest-mass contained in such a disk can be quite large, ranging from $\simeq 0.03\,M_\odot$ in the case of high-mass binaries with stiff equations of state, up to $\simeq 0.2\,M_\odot$ for low-mass binaries with soft equations of state. We comment on the astrophysical implications of our findings and on the long-term evolutionary scenarios that can be conjectured on the basis of our simulations.

Universal Behavior of f_1 and f_{max}

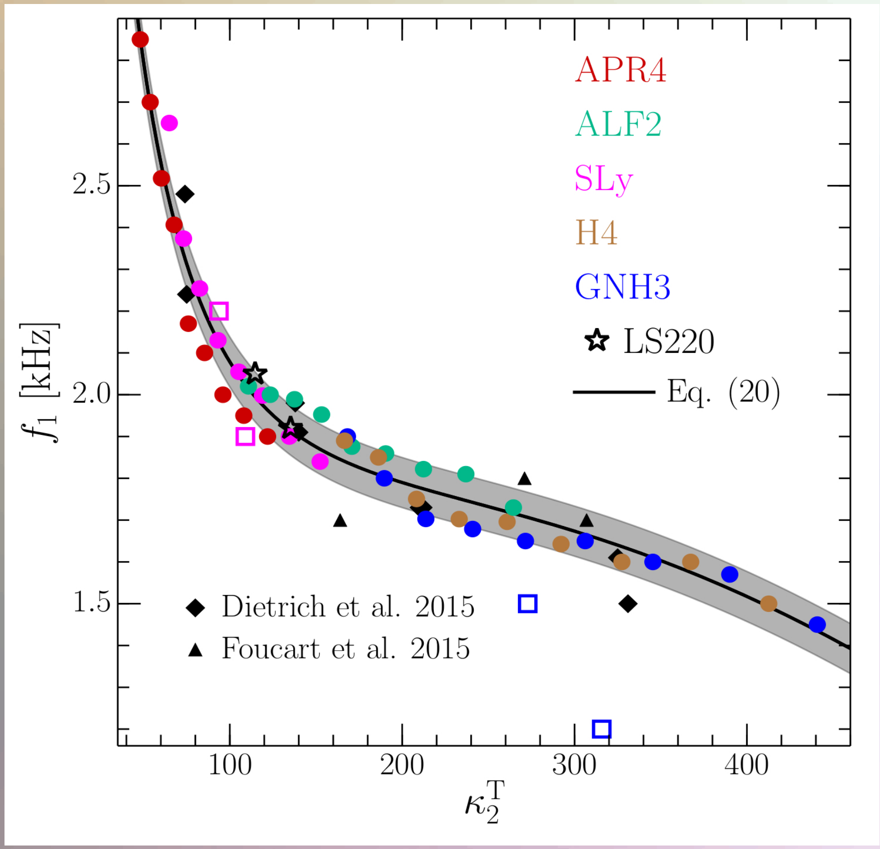

Values of the low-frequency peaks f_1 shown as a function of the tidal deformability parameter κ^T_2.

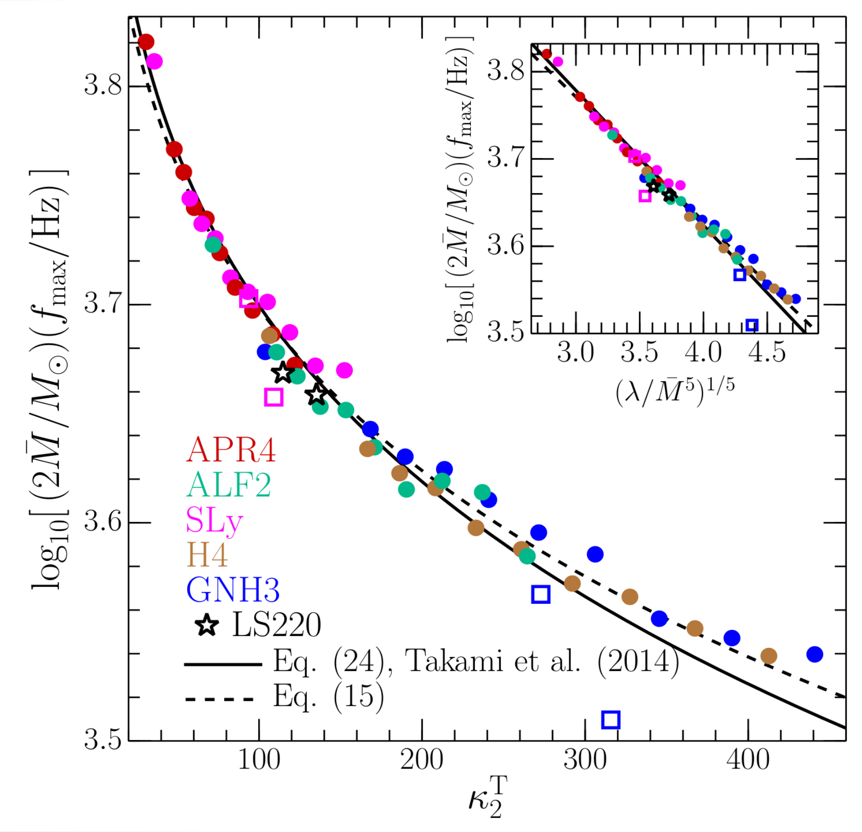

Mass-weighted frequencies at amplitude maximum f_{max} shown as a function of the tidal deformability parameter κ^T_2.

Universal behavior of the f_2-peak

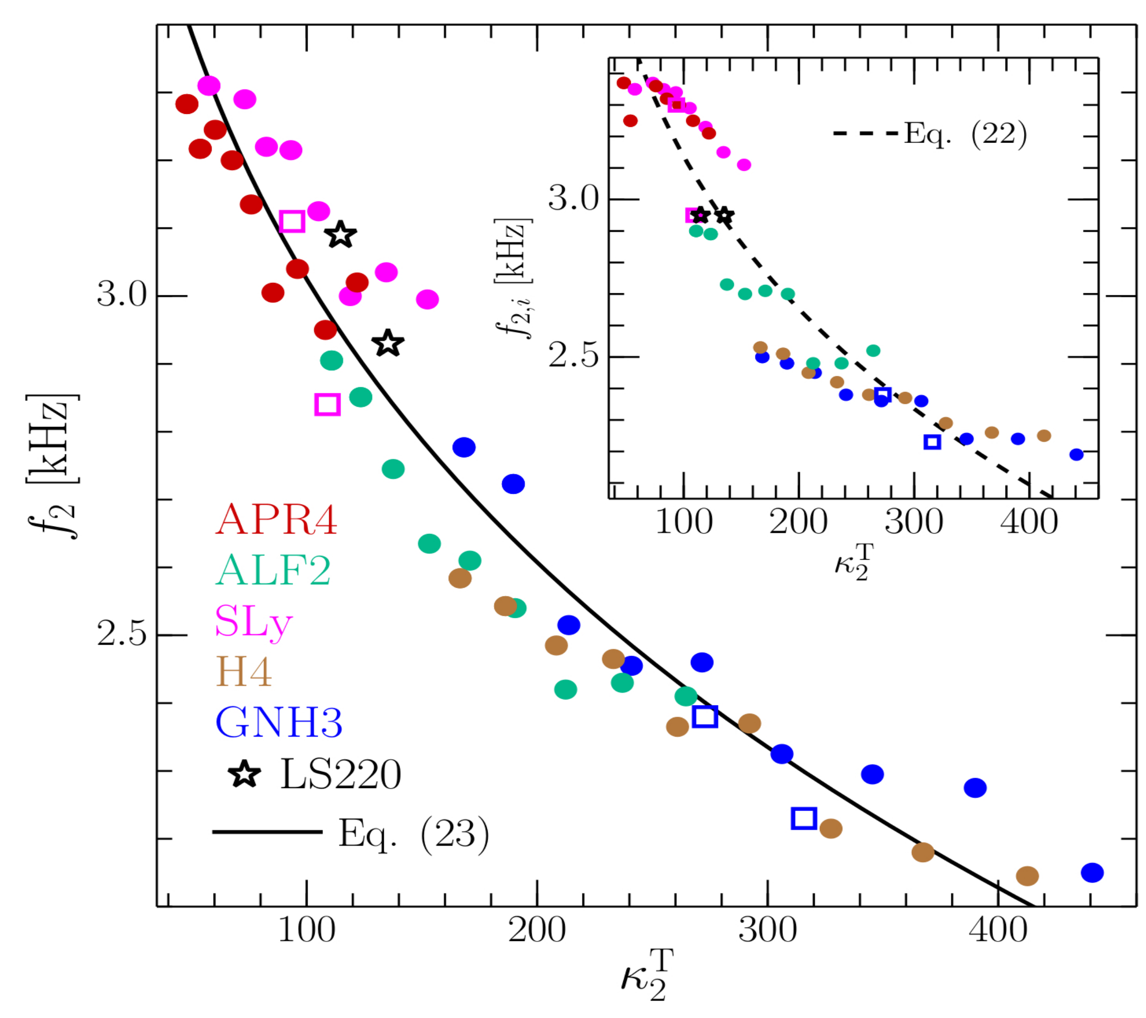

Values of the low-frequency peaks f_2 shown
as a function of the tidal deformability parameter κ^T_2.

Gravitational Waves → Equation of State

The detection of GWs from merging neutron star binaries can be used to determine the high density regime of the EOS. With the knowledge of f_1, f_2 and the total mass the system, the GW signal can set tight constraints on the EOS.

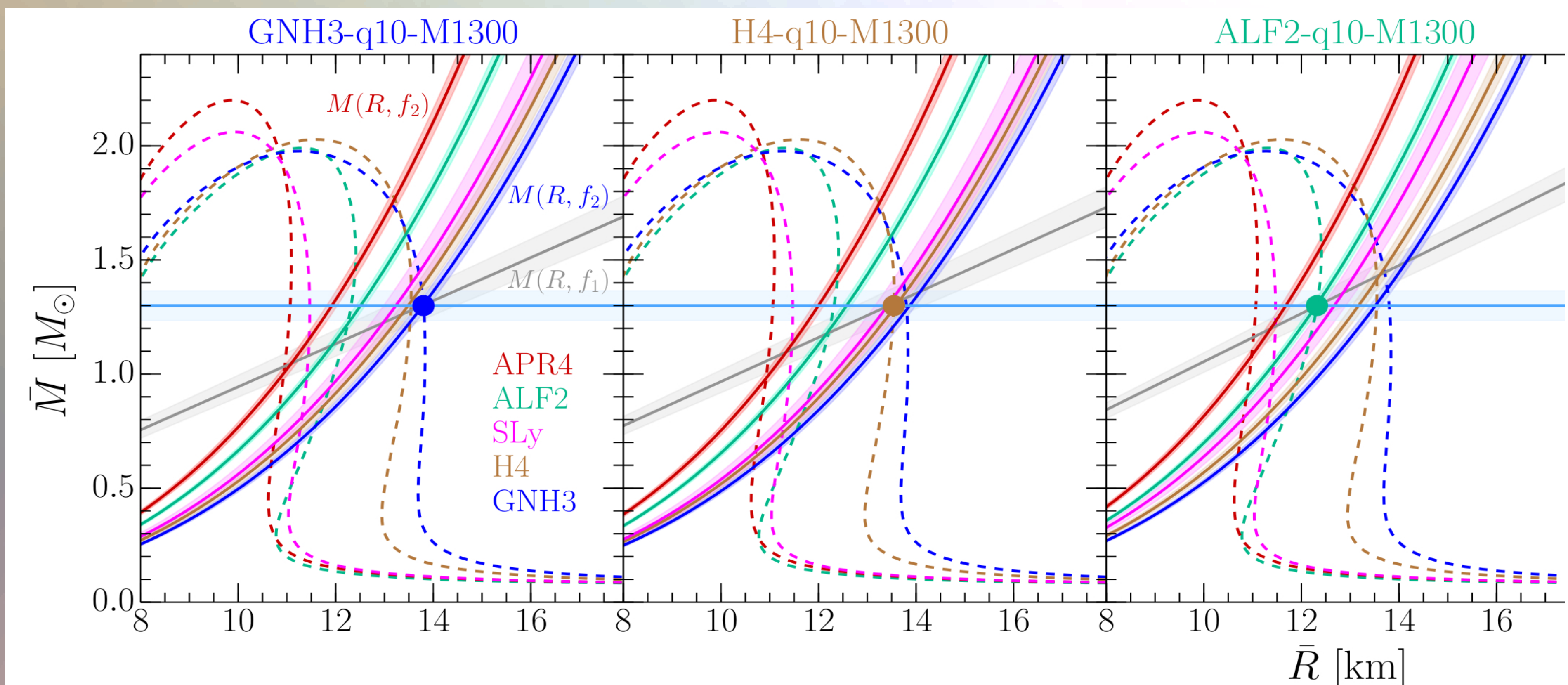

L.Rezzolla and K.Takami, arXiv:1604.00246
K.Takami, L.Rezzolla, and L.Baiotti, Physical Review D 91, 064001 (also PRL 113, 091104)

Gravitational Waves and the maximum of the Rotation Curve

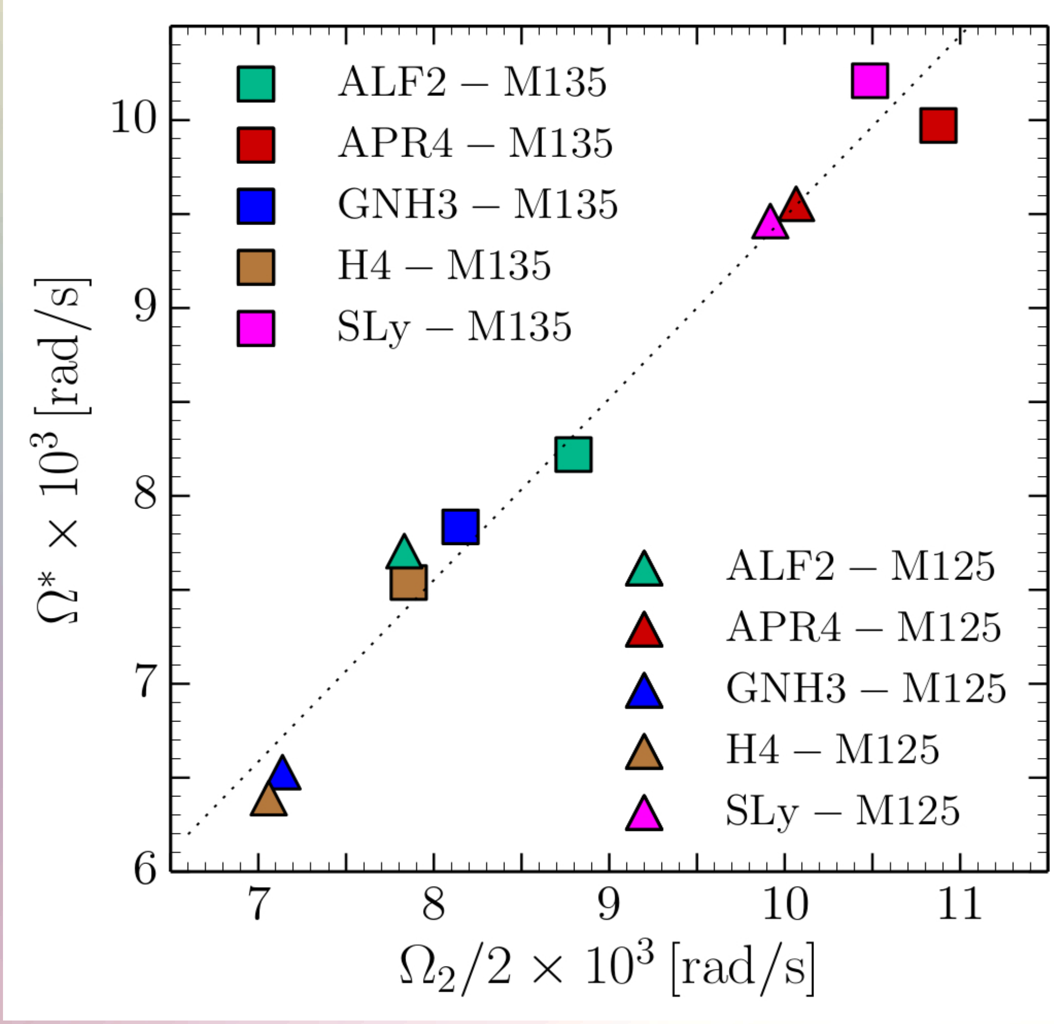

Time-averaged Rotation Profiles

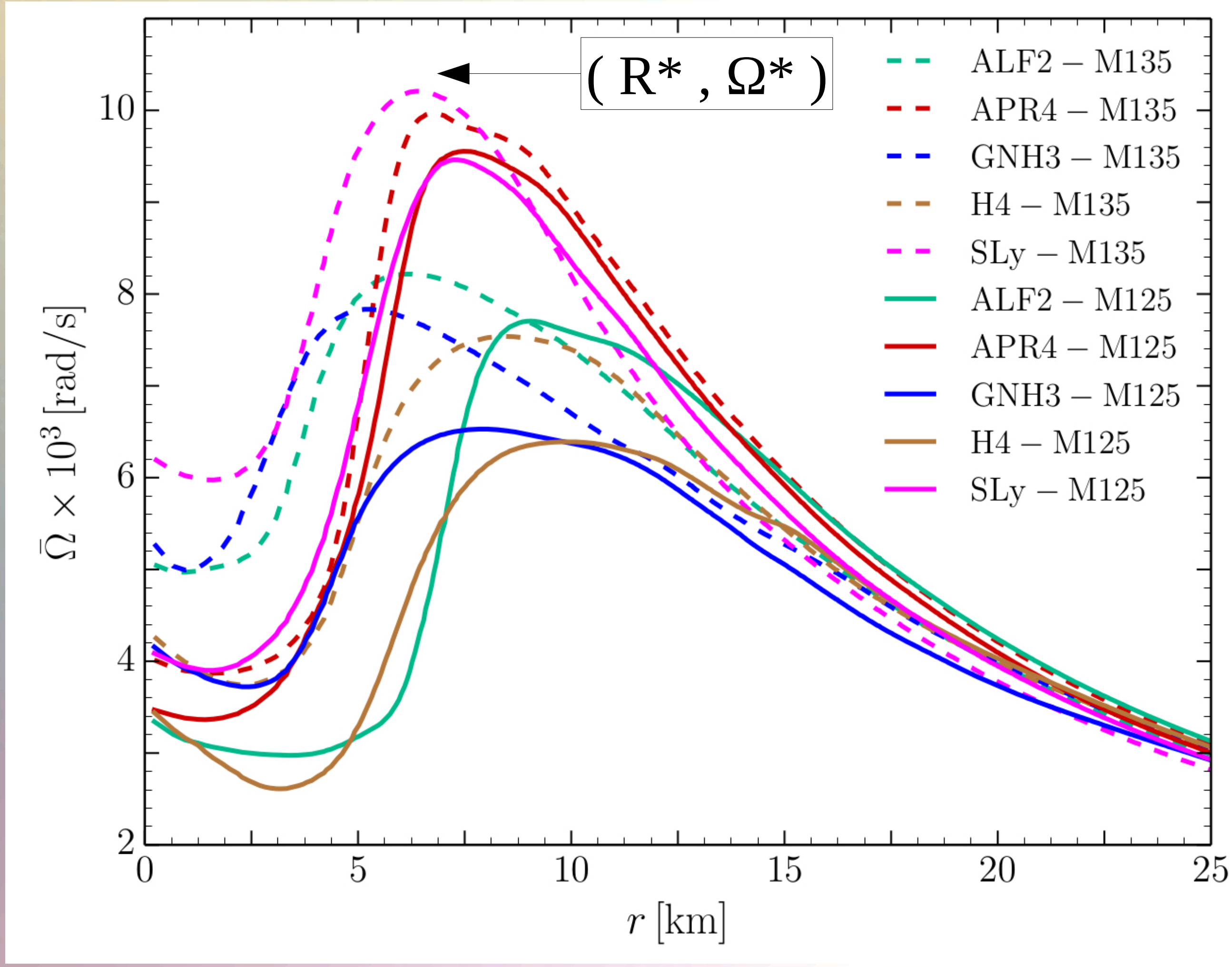

Soft EoSs:
Sly
APR4

Stiff EoSs:
GNH3
H4

Time-averaged rotation profiles for different EoS
Low mass runs (solid curves), high mass runs (dashed curves).

Frame-Dragging and Gravitomagnetism

The dragging of local inertial frames is quite large in the interior of the HMNS and therefore an additional gravitomagnetic force is present. Like the Lorentz-force in electromagnetism, it acts orthogonal to the fluids velocity and the frame dragging.

Ingredients of the angular velocity:

(strong time and φ-dependence !)

$$\Omega(x,y,z,t) = \frac{u^\phi}{u^t} = \alpha\, v^\phi \; - \; \beta^\phi$$

$$\frac{d\mathbf{v}}{d\tau} = -\mathrm{grad}\,\Phi(\mathbf{r}) + 2\,\mathbf{\Omega}^F(\mathbf{r}) \times \mathbf{v} \; + \mathcal{O}(v^2/c^2)\;, \qquad (11)$$

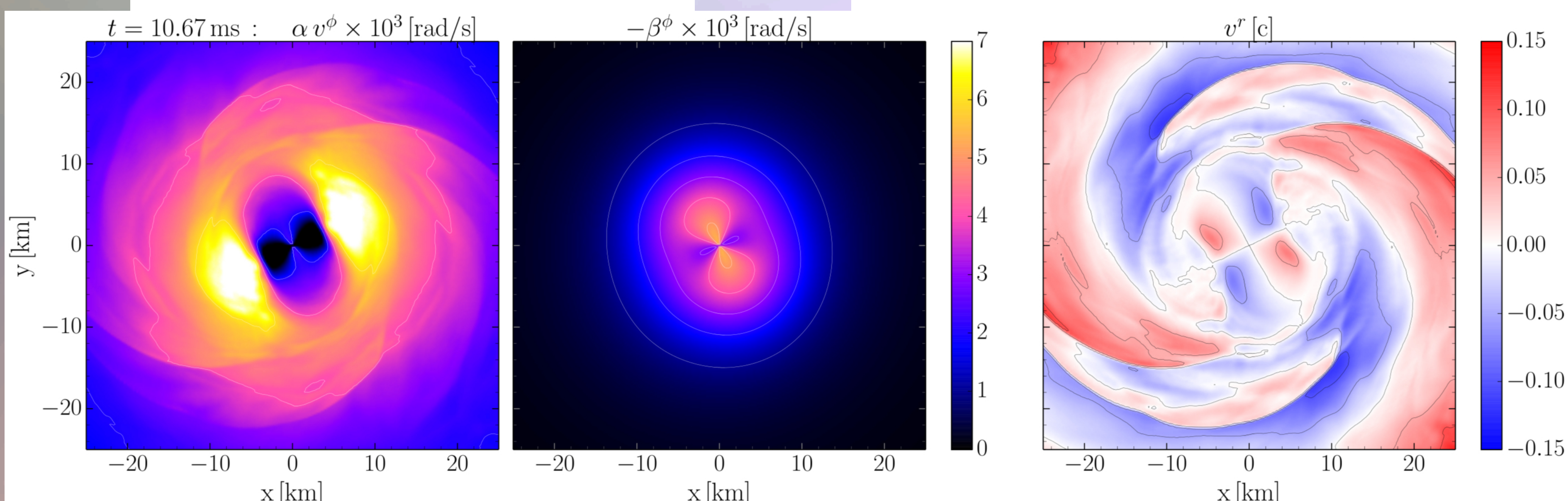

Maximum Value of Ω and its Radial Position (high mass run)

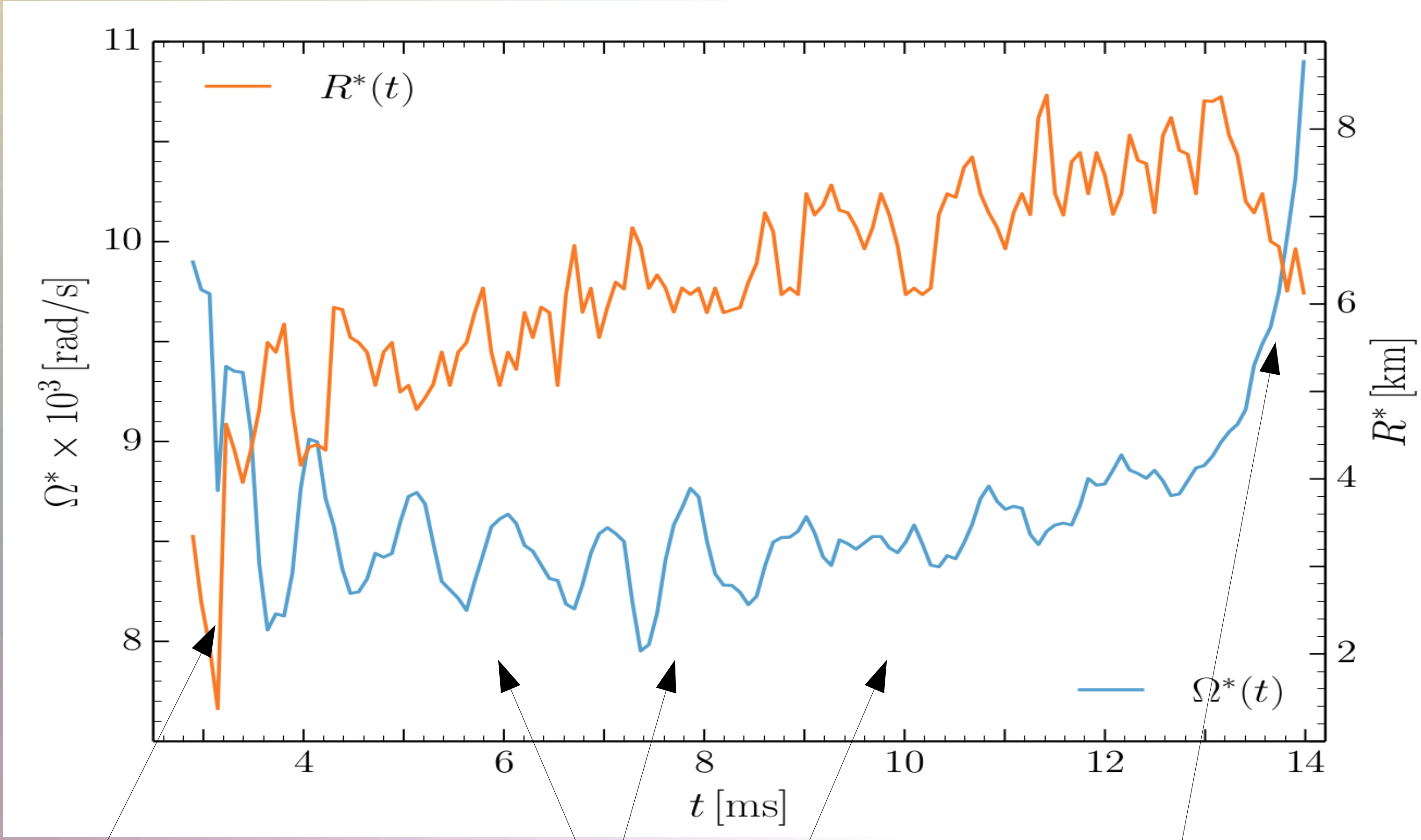

t < 5 ms
Violent early phase

5 ms < t < 13 ms
Gravitomagnetism

Collapse to a black hole

Maximum Value of Ω and its Radial Position (low mass run)

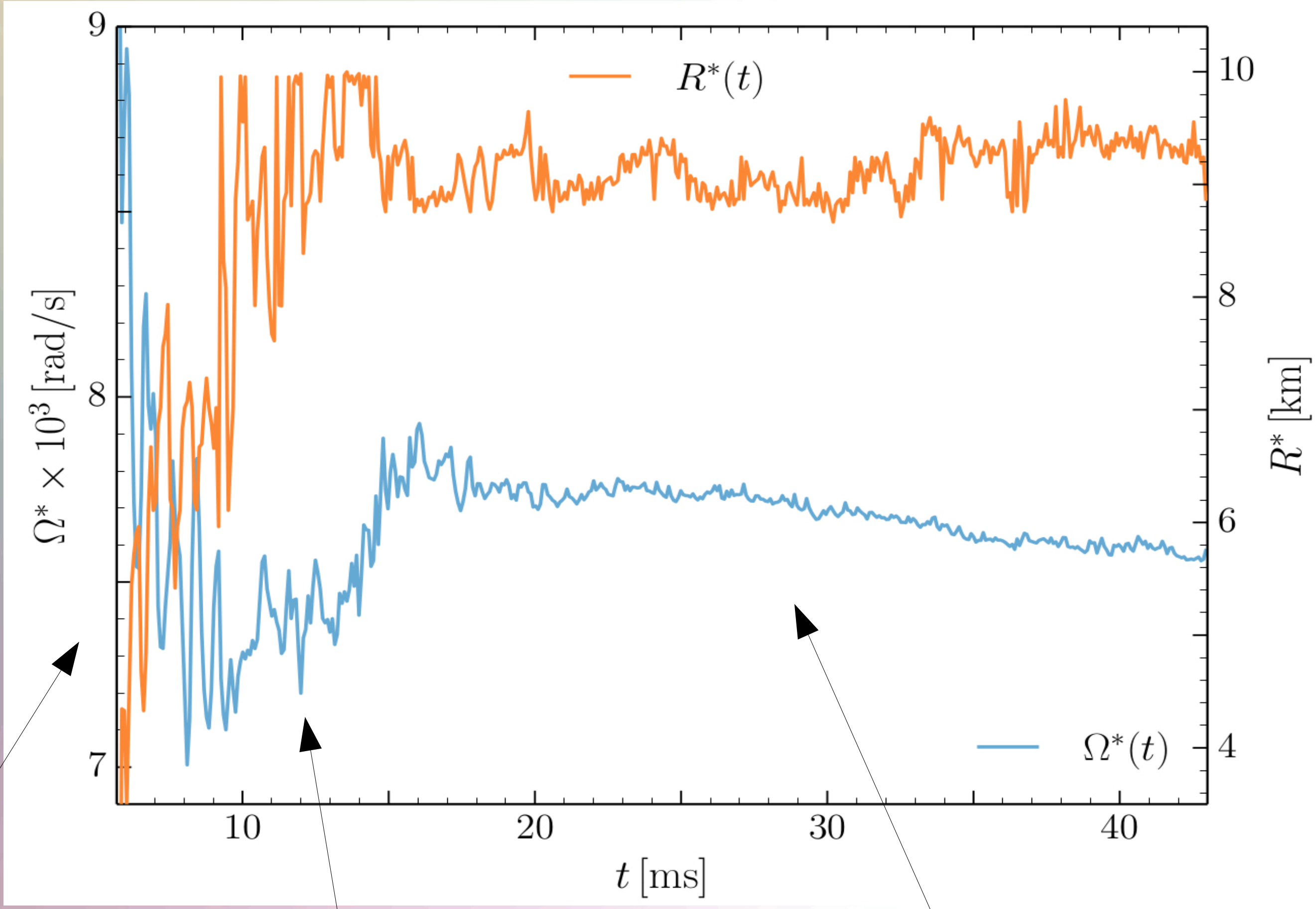

t < 5 ms
Violent early phase

5 ms < t < 15 ms
Gravitomagnetism

t > 15 ms:
Quasi equilibrated and φ-symmetric HMNS

Einstein inside Ausstellung in Frankfurt am Main

Vorlesung: ART mit dem Computer

fias.uni-frankfurt.de/~hanauske/VARTC/

Allgemeine Relativiätstheorie mit dem Computer *von* Dr.phil.nat.Dr.rer.pol. Matthias Hanauske

Home Research Contact

Einführung | Teil I | Teil II | Teil III | *E-Learning*

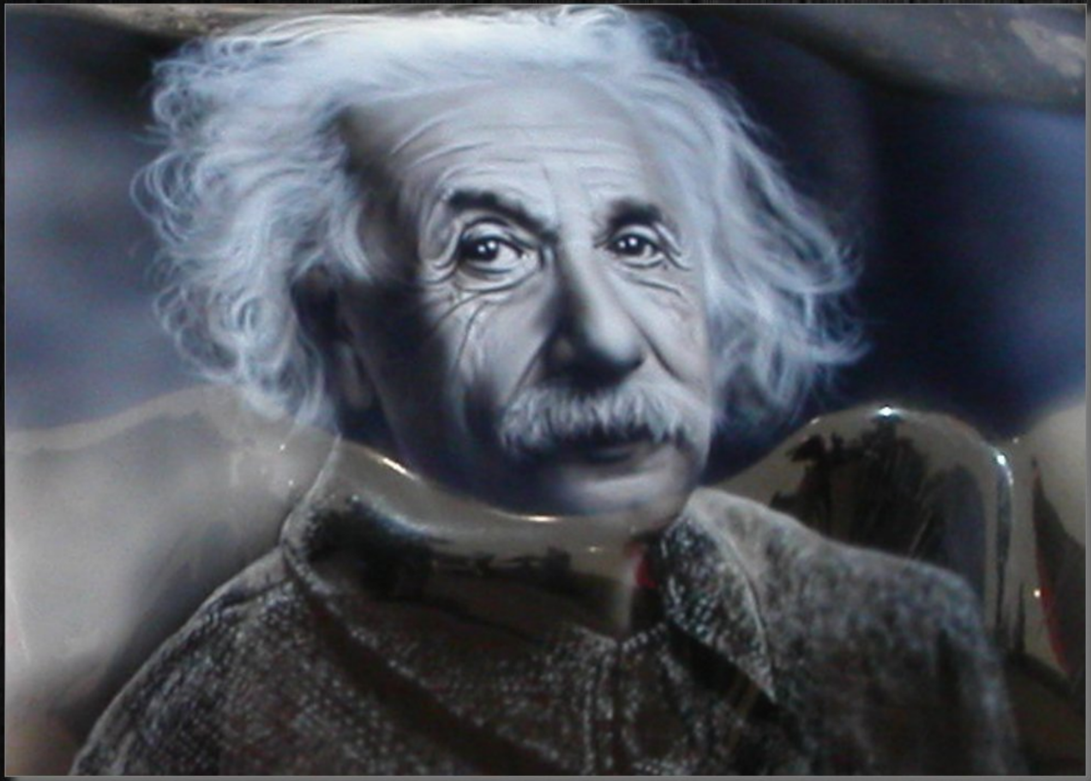

Allgemeine Relativitätstheorie mit dem Computer
(General Theory of Relativity on the Computer)
Vorlesung SS 2016, Mo. 16-18.00 Uhr, PC-Pool 01.120

Zusätzlich zur Vorlesung werden ab dem 18.04.2016 freiwillige Übungstermine eingerichtet, die jeweils montags, eine Stunde vor der Vorlesung im PC-Pool 01.120 stattfinden (Mo. 15-16.00 Uhr).

Am 09.05.2016 findet der Merkur-Transit statt. Im Rahmen der Vorlesung kann der Transit zwischen ca. 13.00 Uhr und 18.30 Uhr vor dem Haupteingang des Instituts für Theoretische Physik beobachtet werden.

In dieser Vorlesung werden die mathematisch anspruchsvollen Gleichungen der Allgemeinen Relativitätstheorie (ART) in diversen Programmierumgebungen analysiert. Im ersten Teil des Kurses erlernen die Studierenden die Verwendung von Computeralgebra-Systemen (Maple und Mathematica). Die oft komplizierten und zeitaufwendigen Berechnungen der tensoriellen Gleichungen der ART können mit Hilfe dieser Programme erleichtert werden. Diverse Anwendungen der Einstein- und Geodätengleichung werden in Maple implementiert, quasi analytische Berechnungen durchgeführt und entsprechende Lösungen berechnet und visualisiert. Der zweite Teil des Kurses befasst sich mit der numerischen Berechnung von Neutronensternen und Weißen Zwergen mittels eines C/C++ Programms. Nach einer kurzen Auffrischung der grundlegenden Programmierkenntnisse, erstellen die Studierenden, gemeinsam mit dem Betreuer, ein Programm, das die Tolman-Oppenheimer-Volkov-Gleichung numerisch löst und visualisieren die Ergebnisse. Zusätzlich wird hierbei in die Grundkonzepte der parallelen Programmierung eingeführt und eine MPI- und OpenMP-Version des C/C++ Programms erstellt. Im dritten Teil des Kurses werden zeitabhängige numerische Simulationen der ART mittels des Einstein Toolkit durchgeführt und deren Ergebnisse mittels Python/Matplotlib visualisiert. Inhaltlich wird hierbei ebenfalls auf den, dem Programm zugrunde liegenden (3+1)-Split der ART

www.fias.uni-frankfurt/~hanauske/VARTC/

Warum (noch) keine Gravitationswellen von kollidierenden Neutronensternen?

Wissenschaftliche Datenaufnahme in 2015

Erste Datenaufnahme

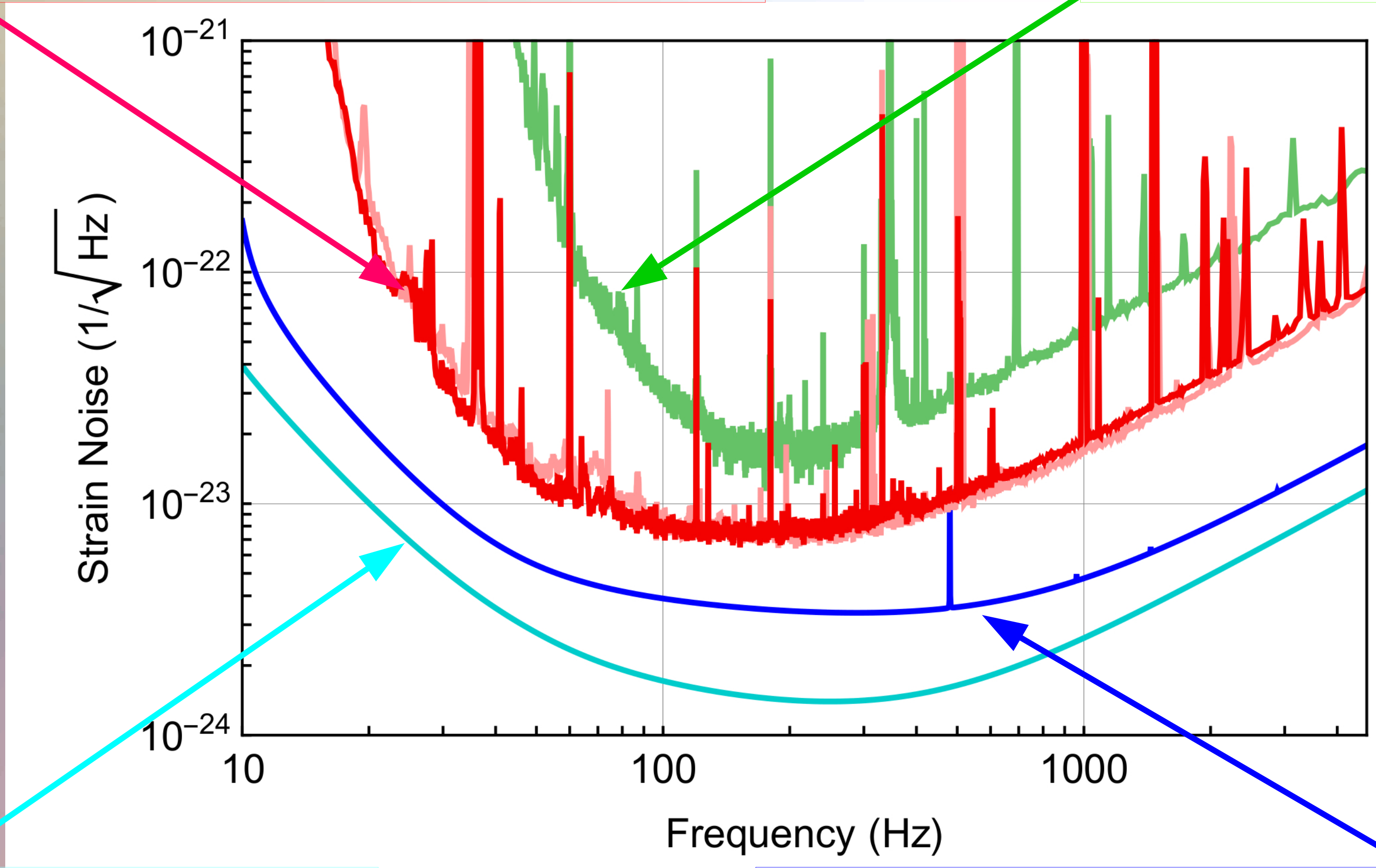

Zukünftige Updates

Nächste Datenaufnahme (Herbst 2016)

The ballroom dance of NS-mergers